Downloaded from rspa.royalsocietypublishing.org on 17 June 2009

PROCEEDINGS OF THE ROYAL SOCIETY A MATHEMATICAL, PHYSICAL & ENGINEERING SCIENCES

Bismuth-Tungsten Oxide Bronzes: A Study of Intergrowth Phases and Related Aspects

A. Ramanan, J. Gopalakrishnan, M. K. Uppal, D. A. Jefferson and C. N. R. Rao

Proc. R. Soc. Lond. A 1984 **395**, 127-139
doi: 10.1098/rspa.1984.0093

Email alerting service

Receive free email alerts when new articles cite this article - sign up in the box at the top right-hand corner of the article or click **here**

To subscribe to *Proc. R. Soc. Lond. A* go to:
http://rspa.royalsocietypublishing.org/subscriptions

This journal is © 1984 The Royal Society

Downloaded from rspa.royalsocietypublishing.org on 17 June 2009

Proc. R. Soc. Lond. A **395**, 127–139 (1984)
Printed in Great Britain

Bismuth–tungsten oxide bronzes: a study of intergrowth phases and related aspects

By A. Ramanan[1], J. Gopalakrishnan[1], M. K. Uppal[2], D. A. Jefferson[2] and C. N. R. Rao, F.R.S.[1,2]

[1] *Solid State and Structural Chemistry Unit, Indian Institute of Science, Bangalore-560012, India*

[2] *Department of Physical Chemistry, University of Cambridge, Cambridge CB2 1EP, U.K.*

(*Received* 24 *January* 1984)

[Plates 1–10]

Reaction of bismuth metal with WO_3 in the absence of oxygen yields interesting bronze-like phases. From analytical electron microscopy and X-ray photoelectron spectroscopy, the product phases are found to have the general composition Bi_xWO_3 with bismuth in the 3+ state. Structural investigations made with high resolution electron micrscopy and cognate techniques reveal that when $x < 0.02$, a perovskite bronze is formed. When $x \geqslant 0.02$, however, intergrowth tungsten bronzes (i.t.b.) containing varying widths of the WO_3 slab are formed, the lattice periodicity being in the range 2.3–5.1 nm in a direction perpendicular to the WO_3 slabs. Image-matching studies indicate that the bismuth atoms are in the tunnels of the hexagonal tungsten bronze (h.t.b.) strips and the h.t.b. strips always remain one-tunnel wide. Annealed samples show a satellite structure around the superlattice spots in the electron diffraction patterns, possibly owing to ordering of the bismuth atoms in the tunnels. The i.t.b. phases show recurrent intergrowths extending up to 100 nm in several crystals. The periodicity varies considerably within the same crystal wherever there is disordered intergrowth, but unit cell dimensions can be assigned from X-ray and electron diffraction patterns. The maximum value of x in the i.t.b. phases is *ca.* 0.07 and there is no evidence for the i.t.b. phase progressively giving way to the h.t.b. phase with increase in x. Hexagonal tungsten bronzes that contain bismuth with x up to 0.02 can be formed by starting from hexagonal WO_3, but the h.t.b. phase seems to be metastable. Optical, magnetic and electron transport properties of the i.t.b. phases have been measured and it appears that the electrons become itinerant when $x > 0.05$.

1. Introduction

Bismuth forms two tungstates, Bi_2WO_6 and $Bi_2W_2O_9$. The third member of this homologus series, $Bi_2W_nO_{3n+3}$, has not been isolated as a single phase material, but $Bi_2W_3O_{12}$ is found occasionally as an intergrowth in $Bi_2W_2O_9$ (Jefferson *et al.* 1982). These homologous tungstates are similar to the well known Aurivillius

The Royal Society is collaborating with JSTOR to digitize, preserve, and extend access to *Proceedings of the Royal Society of London. Series A, Mathematical and Physical Sciences.* www.jstor.org

Downloaded from rspa.royalsocietypublishing.org on 17 June 2009

phases (Aurivillius 1949; Hutchinson *et al.* 1977, $Bi_2A_{n-1}M_nO_{3n+3}$ (A = Ba, Bi; M = Ti, W, Nb), except that instead of the $A_{n-1}M_nO_{3n+1}$ perovskite layers, W_nO_{3n+1} layers are present in between Bi_2O_2 layers in the tungstates. We considered it worthwhile to investigate the interaction between bismuth metal and WO_3 to see if reduced forms of the homologous tungstates of the type $Bi(WO_3)_n$ are formed. If such compounds are indeed formed, they can be solid solutions of the type $Bi_xW_{1-x}O_{3-y}$ or tungsten bronzes of the general formula Bi_xWO_3. The bronzes can be perovskite-like, tetragonal, hexagonal or, more interestingly, of the intergrowth variety. In spite of the extensive studies on tungsten bronzes reported in the literature, the Bi–WO_3 system has not been examined in any detail before and we have now made a detailed investigation of this system by using high resolution electron microscopy, X-ray diffraction and other techniques.

Various types of bronze structures have been reviewed by Ekstrom & Tilley (1980) and the structural principles of intergrowth bronzes have been discussed by Hussain & Kihlborg (1976). Intergrowth tungsten bronzes (i.t.b.) are characterized by the intergrowth of WO_3 slabs and strips of the hexagonal tungsten bronze (h.t.b.) structure. The i.t.b. phases described in the literature are rarely ordered, even on an ultramicrostructural scale, and the widths of the WO_3 slabs display a considerable variation, the h.t.b. regions ranging from one to three tunnels in width. The present study has shown that bismuth forms novel intergrowth bronze phases with wide-ranging periodicities, but with the h.t.b. region always limited to one tunnel in width. Bismuth atoms occupy the hexagonal tunnels and the maximum value of x in Bi_xWO_3 appears to be *ca.* 0.10. We see no evidence for the i.t.b. phase giving way to the h.t.b. phase at large x. Recurrent coherent intergrowth in the i.t.b. phases extends up to 100 nm in some of the crystals and the largest cell parameter varies between 2 and 5 nm. More significantly, the present study on this i.t.b. system is probably the only one where ultrastructural studies have been made on samples that are well characterized, including *in situ* analysis. Results of the present study along with the observations on other coherent intergrowth systems in the recent literature raise questions about the traditional definitions of a phase and a unit cell. H.t.b. phases of bismuth ($x < 0.1$) prepared independently by starting from hexagonal WO_3 have a random distribution of bismuth atoms and seem to be metastable. Futhermore, h.t.b. phases with $x > 0.10$ cannot be made. In all the bronzes, bismuth is present in the 3+ state, each bismuth atom donating three electrons to WO_3. Accordingly, the electrical resistivity of i.t.b. Bi_xWO_3 phases decreases with increase in x, the d electrons becoming itinerant when $x > 0.05$.

2. Experimental

Samples of Bi_xWO_3 for nominal x values of 0.01, 0.02, 0.05, 0.1 and 0.2 were prepared by heating WO_3 with metallic bismuth in the appropriate proportions in sealed and evacuated silica tubes at 1170 K for periods of six days. Initial characterization was by X-ray powder diffractometry employing a Philips diffractometer.

Samples were prepared for the electron microscope by liquid nitrogen embrittle-

Downloaded from rspa.royalsocietypublishing.org on 17 June 2009

ment, followed by grinding in acetone suspension and deposition onto holey carbon films. Micrographs of regions of interest were recorded at magnifications in the range $\times 300\,000 - \times 600\,000$, astigmatism being corrected by observing the granularity of the holey carbon support film. Selected area electron diffraction (s.a.e.d) patterns were also recorded from the areas studied.

For the initial h.r.e.m. studies, samples were examined in a JEM-200CX electron microscope fitted with a side-entry goniometer and energy-dispersive X-ray detector. When operated at 200 kV, the objective lens characteristics of the instrument ($C_s = 2.8$ mm, $C_c = 3.4$ mm) were such that the interpretable point resolution just below the so-called Scherzer focus was of the order of 0.289 nm (figure 1*a*).

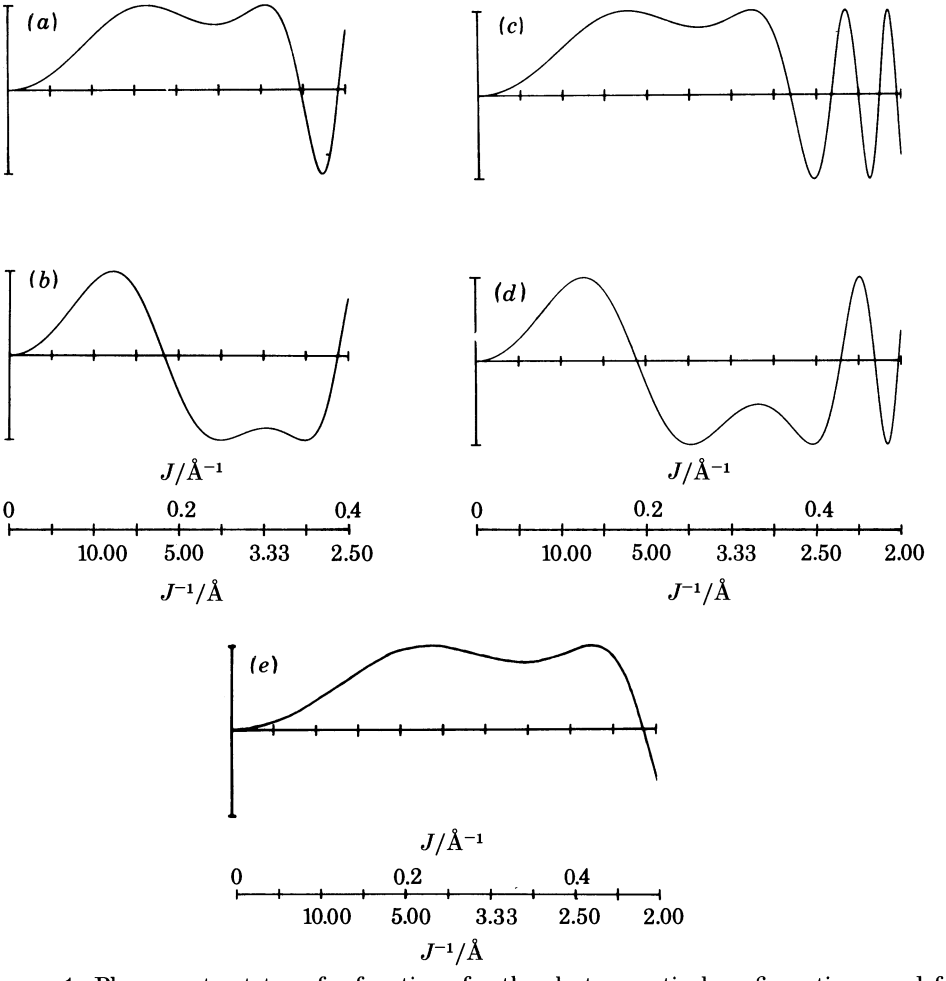

FIGURE 1. Phase contrast transfer functions for the electron-optical configurations used for image: (*a*) 200CX, initial configuration, $\Delta f = 85$ nm; (*b*) $\Delta f = 135$ nm; (*c*) 200CX, later configuration, $\Delta f = 72$ nm; (*d*) $\Delta f = 122$ nm; (*e*) Cambridge h.r.e.m., $\Delta f = 70$ nm. In all cases, the chromatic–beam divergence envelope is not shown because the conditions of validity of this approximation were not met in the actual images recorded.†

† 1 Å $= 10^{-10}$ m $= 0.1$ nm.

Downloaded from rspa.royalsocietypublishing.org on 17 June 2009

Considering a simple damping envelope on the p.c.t.f. to indicate the effects of chromatic aberration and beam divergence (Fejes 1977), it could readily be shown that resolution up to *ca.* 0.25 nm was possible although this approximation was not directly applicable in the imaging conditions used. Consequently, most micrographs were recorded at a defocus well below the Scherzer position (figure 1*b*), to utilize the available resolution. Under such conditions, however, the atomic detail was imaged with reversed contrast and the p.c.d. approximation (Lynch *et al.* 1975) could not be used in image interpretation, image-matching studies using the multislice method (Goodman & Moodie 1974) being necessary. For a later part of the investigation the objective lens characteristics were improved to $C_s = 1.9$ mm and $C_c = 1.9$ mm. The corresponding 'optimum' and 'most useful' transfer function conditions for this later configuration are shown in figure 1*c*, *d*. To confirm the final model of the structure, images of the $Bi_{0.1}WO_3$ sample were recorded at 500 kV by using the Cambridge University high resolution electron microscope (h.r.e.m.) (Smith *et al.* 1982). In this case there was no advantage in going beyond the 'optimum' focus position (figure 1*e*), which was therefore used throughout. The interpretable point resolution of the images obtained was then of the order of 0.2 nm.

X-ray photoelectron spectra were recorded with a VG Escalab instrument using Mg Kα radiation. The W (4f) signal was monitored with polycrystalline samples (Rao *et al.* 1979) and the relative intensities of W^{5+} and W^{6+} peaks were reproducible. The intensities were obtained by decomposing the 4f peaks into two Gaussians after subtracting the background. Reflectance spectra were measured with a Pye-Unicam SP8-100 spectrometer with MgO used as reference. Electrical resistivities were measured by the four-probe technique on pressed pellets of near-theoretical density. Seebeck coefficient measurements were made with a 'home-built' apparatus, while the magnetic measurements were made by the Faraday method with use of a Cahn electrobalance.

3. Results and discussion

Characterization

Interaction of bismuth with WO_3 can give rise to $Bi_xW_{1-x}O_{3-y}$ or bronze-like Bi_xWO_3, depending on whether bismuth is in the 5+ or the 3+ state. In $Bi_xW_{1-x}O_{3-y}$, Bi^{5+} would substitute for W^{6+}, while in Bi_xWO_3, Bi^{3+} would occupy interstitial sites in WO_3. X-ray photoelectron spectra in the Bi(4f) region (figure 2) clearly show that bismuth is present in the 3+ state. Accordingly, the W(4f) spectra (figure 3) show the presence of both W^{5+} and W^{6+} states, the presence of each bismuth atom requiring three W^{5+} ions. These observations suggest that the products of the reaction of Bi with WO_3 are most likely to be bronze-like. A scanning electron microscope examination showed that Bi_xWO_3 samples with $x \geqslant 0.05$ exhibit a plate-like habit, while samples with $x < 0.05$ show a three-dimensional habit similar to WO_3 (figure 4, plate 1). As expected of bronzes, the Bi_xWO_3 samples exhibit intense colours ranging from green to blue–black.

X-ray powder diffraction patterns of the $x = 0.01$ sample could be indexed on an orthorhombic unit cell with $a = 0.737(1)$, $b = 0.748(1)$ and $c = 0.3856(8)$ nm.

Downloaded from rspa.royalsocietypublishing.org on 17 June 2009

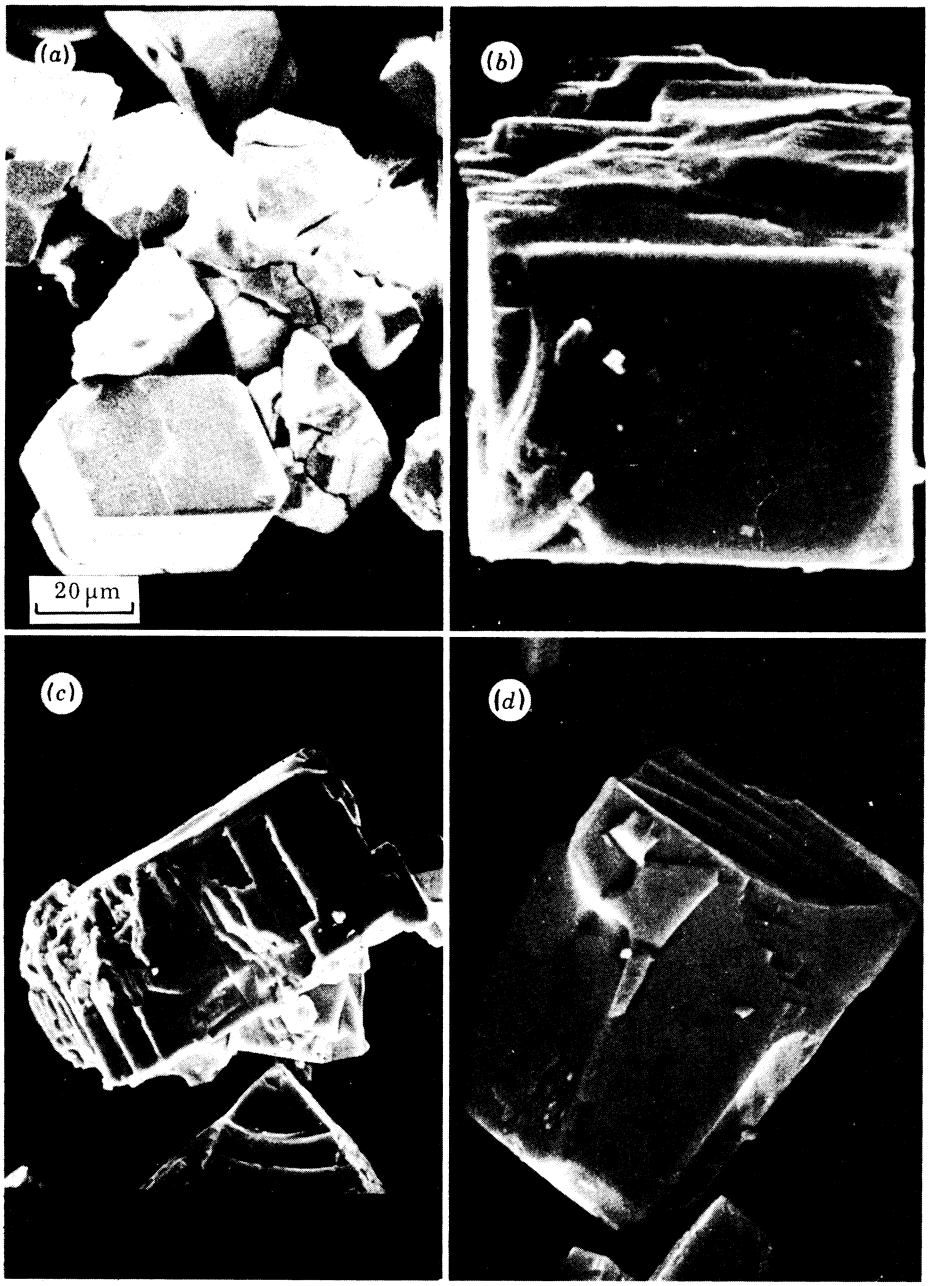

FIGURE 4. Scanning electron micrographs of Bi_xWO_3: (*a*) $x = 0.01$; (*b*) and (*c*) $x = 0.05$ and (*d*) $x = 0.10$. Magnifications are (*a*) ×2000, (*b*) ×2000, (*c*) ×1000 and (*d*) ×5000.

(*Facing p.* 130)

Downloaded from rspa.royalsocietypublishing.org on 17 June 2009

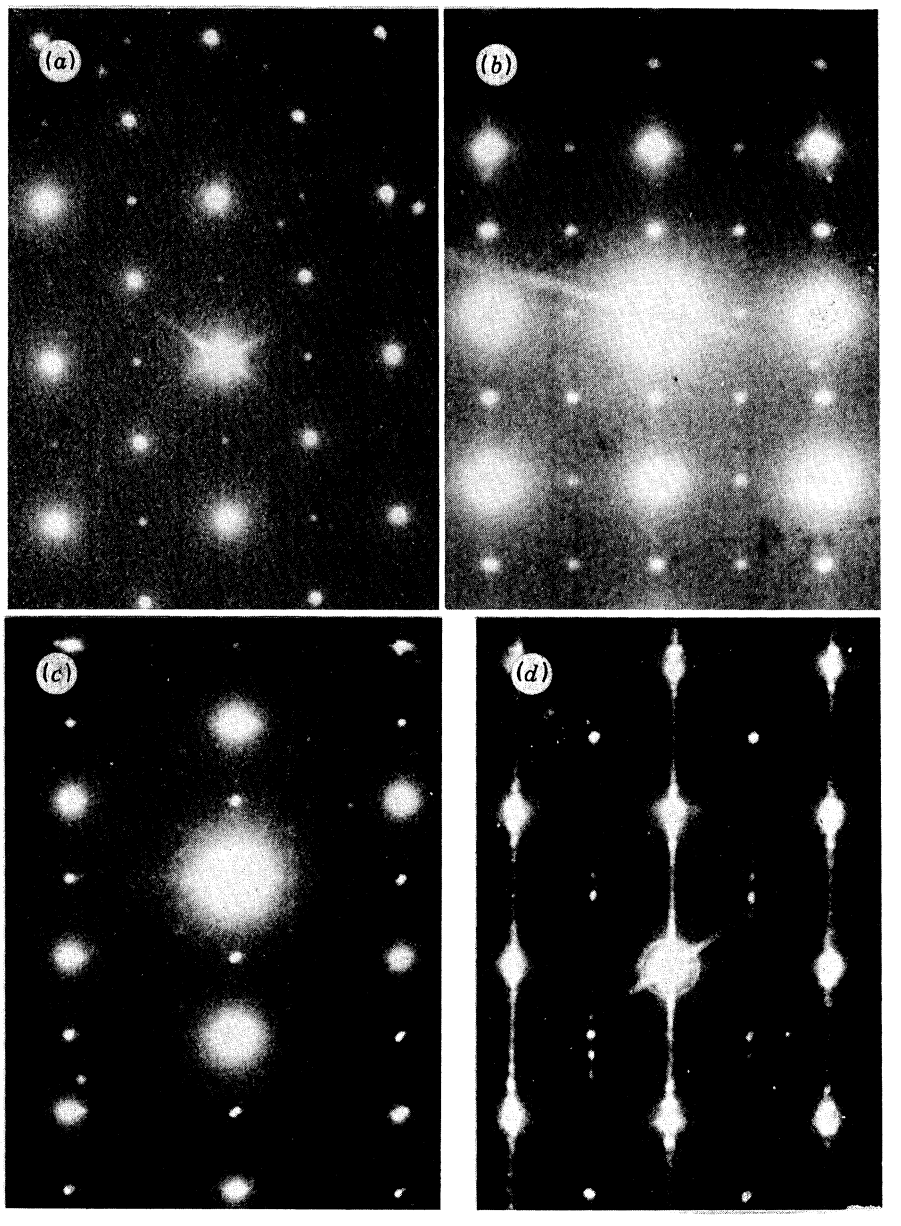

FIGURE 5. Electron diffraction patterns of WO_3-like crystals of $Bi_{0.01}WO_3$. Electron beam parallel to $[0\bar{1}0]$ in (*a*), [001] in (*b*) and $[01\bar{1}]$ in (*c*). The pattern of a minor phase showing streaking along a^* is shown in (*d*).

Downloaded from rspa.royalsocietypublishing.org on 17 June 2009

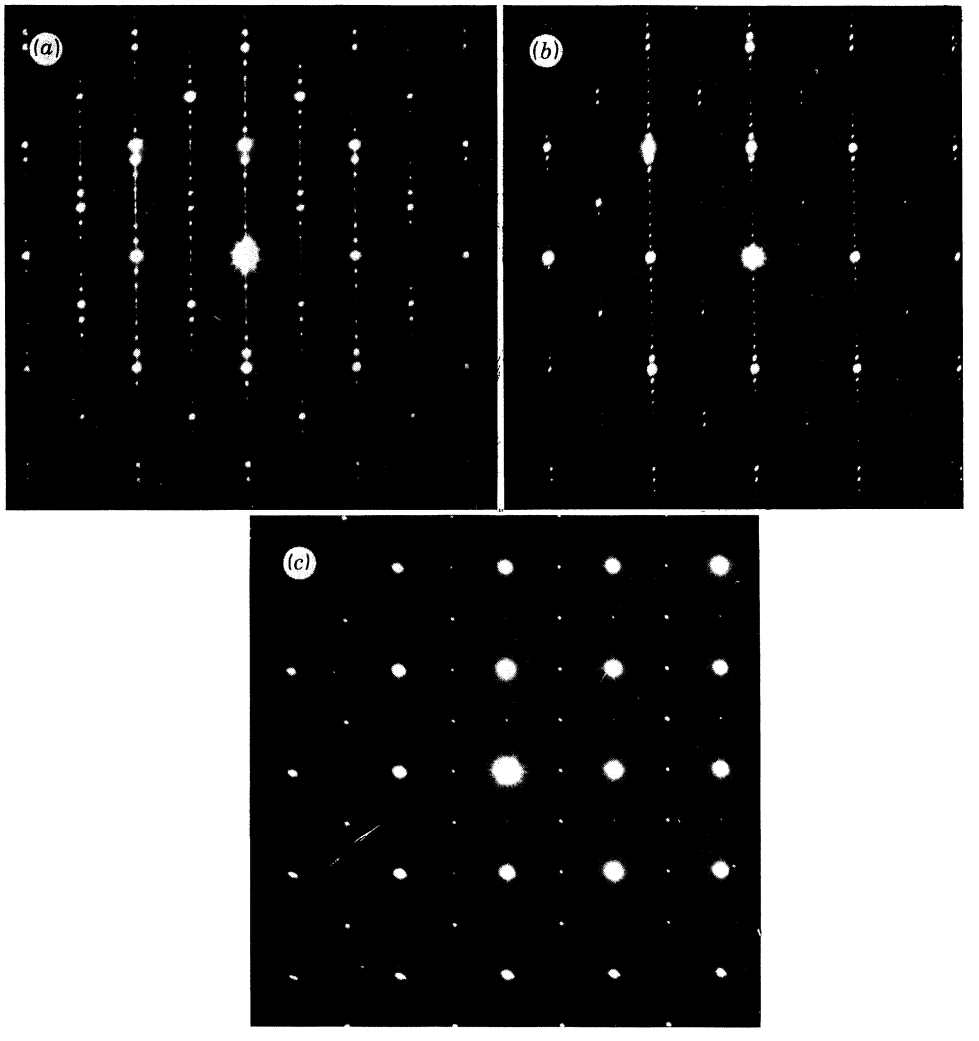

FIGURE 6. Typical s.a.e.d patterns of Bi–W-bronzes: (*a*) and (*b*) are principal sections showing the one-dimensional superlattice. These correspond to projection down [001] and [010] respectively, by the nomenclature of Hussain & Kihlborg (1976); (*c*) is the projection down the [100] axis.

Downloaded from rspa.royalsocietypublishing.org on 17 June 2009

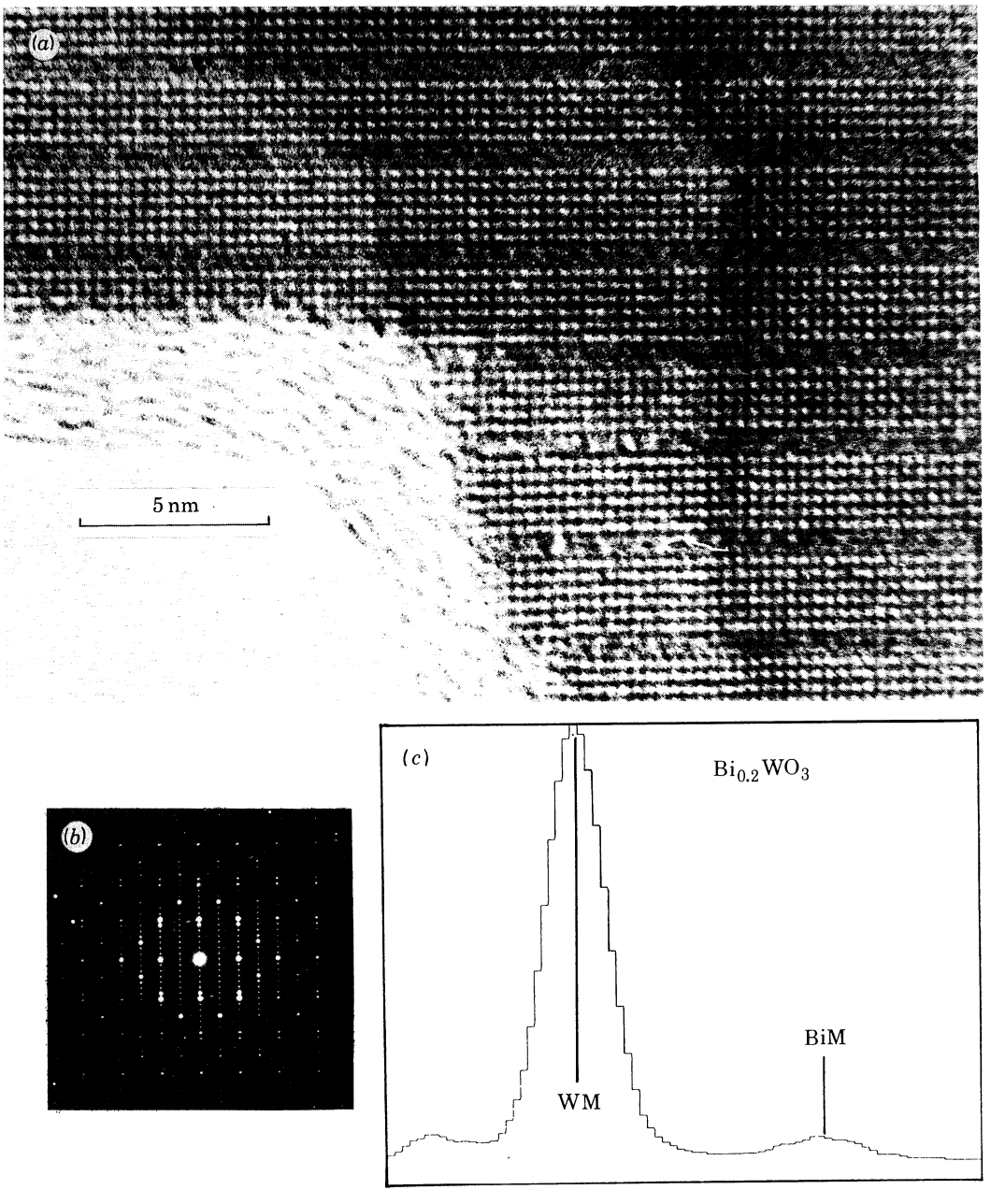

FIGURE 7. (*a*) h.r.e.m. (200 kV) image; (*b*) s.a.e.d. pattern and (*c*) part of the X-ray emission spectrum of a crystal of nominal composition of $Bi_{0.2}WO_3$. The image corresponds to the [001] projection.

Downloaded from rspa.royalsocietypublishing.org on 17 June 2009

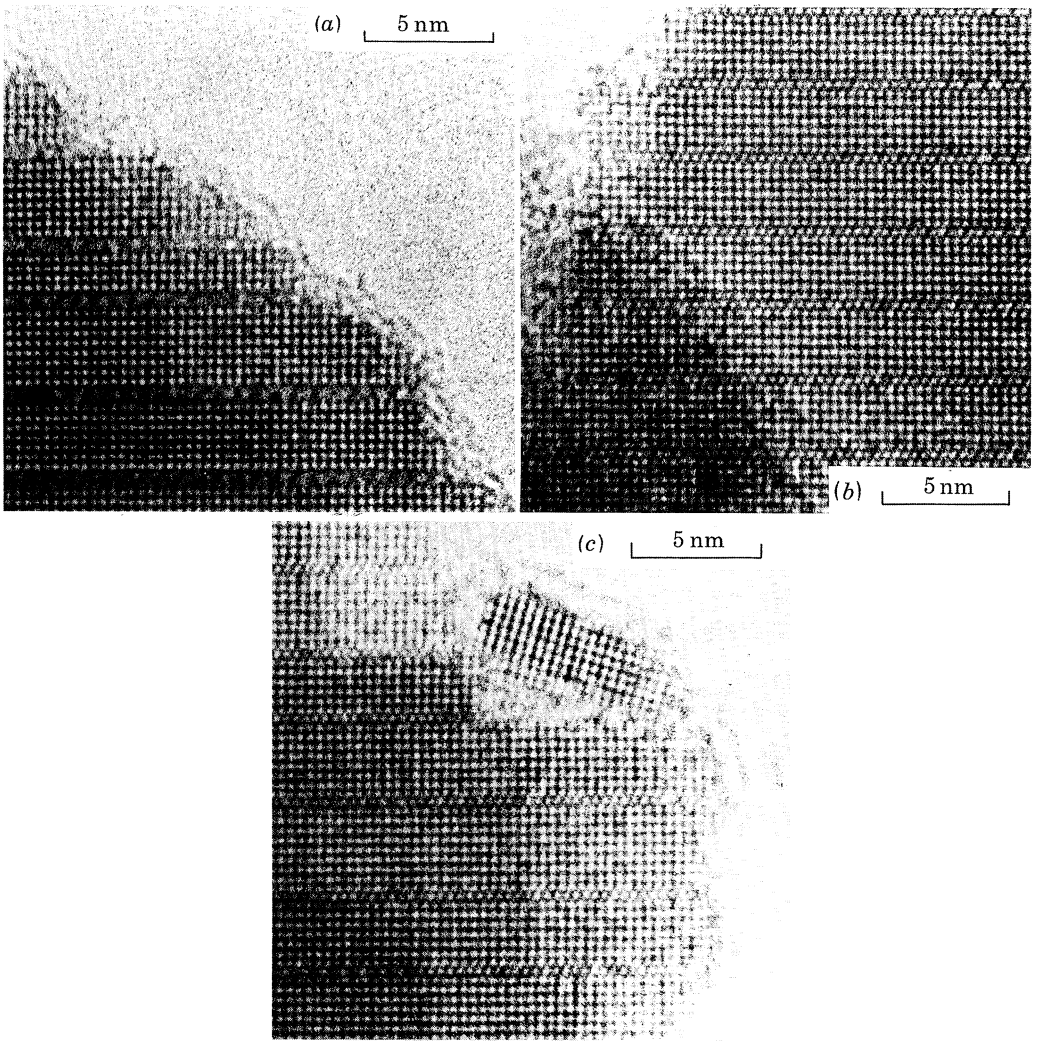

FIGURE 9. (*a*) H.r.e.m. image of a disordered intergrowth bronze of nominal composition $Bi_{0.1}WO_3$, $\Delta f \approx 150$ nm; (*b*) a more ordered crystal in the same sample, $\Delta f = 120$ nm; (*c*) crystal showing fragmentation at the edge, $\Delta f = 120$ nm. Axis of projection in each case is [001].

Downloaded from rspa.royalsocietypublishing.org on 17 June 2009

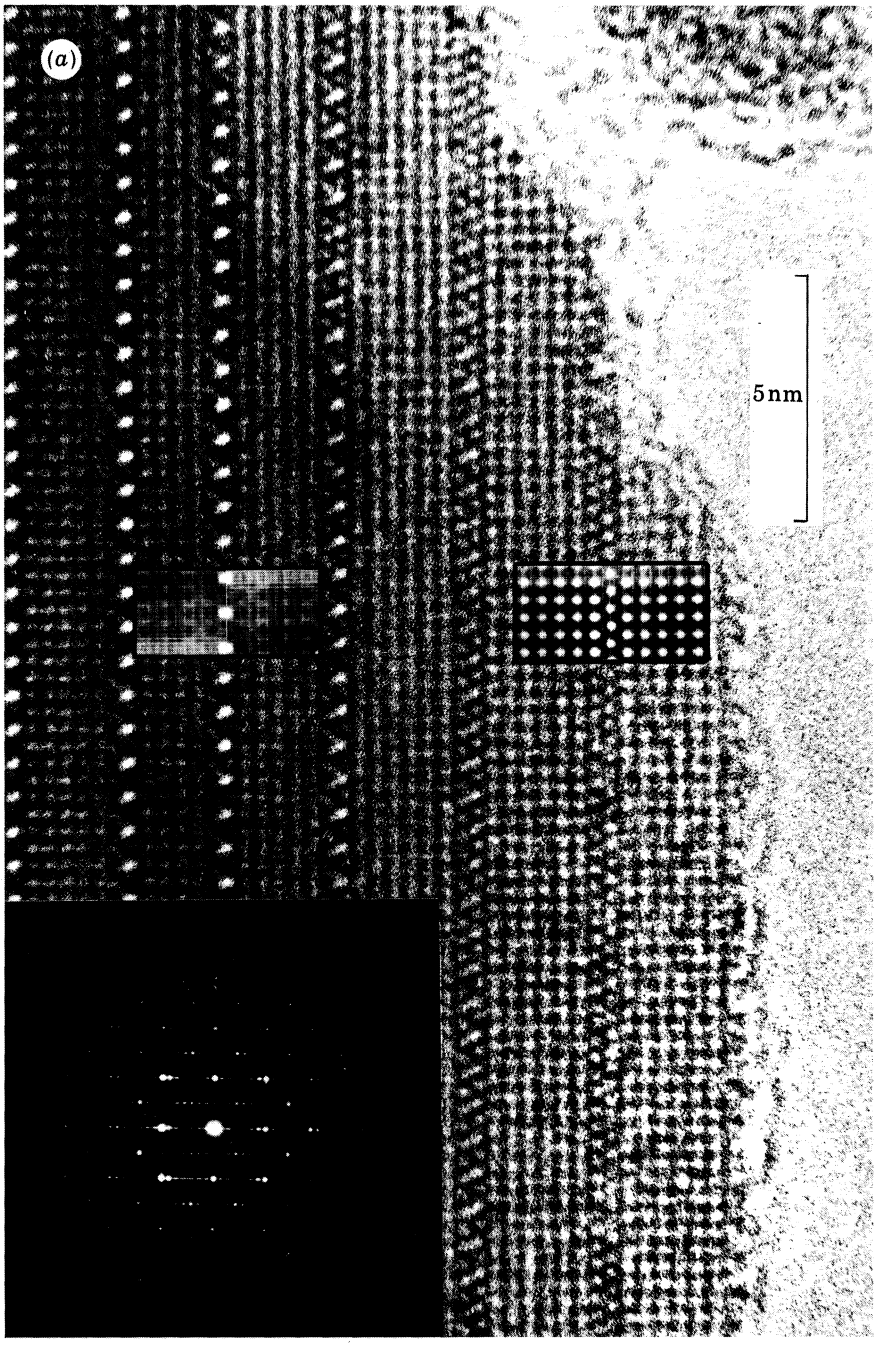

FIGURE 11. Image matching studies for the sample of nominal composition $Bi_{0.1}WO_3$. (*a*) [001] projection, simulations (inset) for crystal thickness of 3 nm (near edge) and 6 nm, $\Delta f = 120$ nm; (*b*) (opposite) [010] projection, simulation for crystal thickness of 4.5 nm and $\Delta f = 120$ nm. Completely filled tunnels in the simulations correspond to composition of $Bi_{0.067}WO_3$. The corresponding s.a.e.d. patterns are also shown.

Downloaded from rspa.royalsocietypublishing.org on 17 June 2009

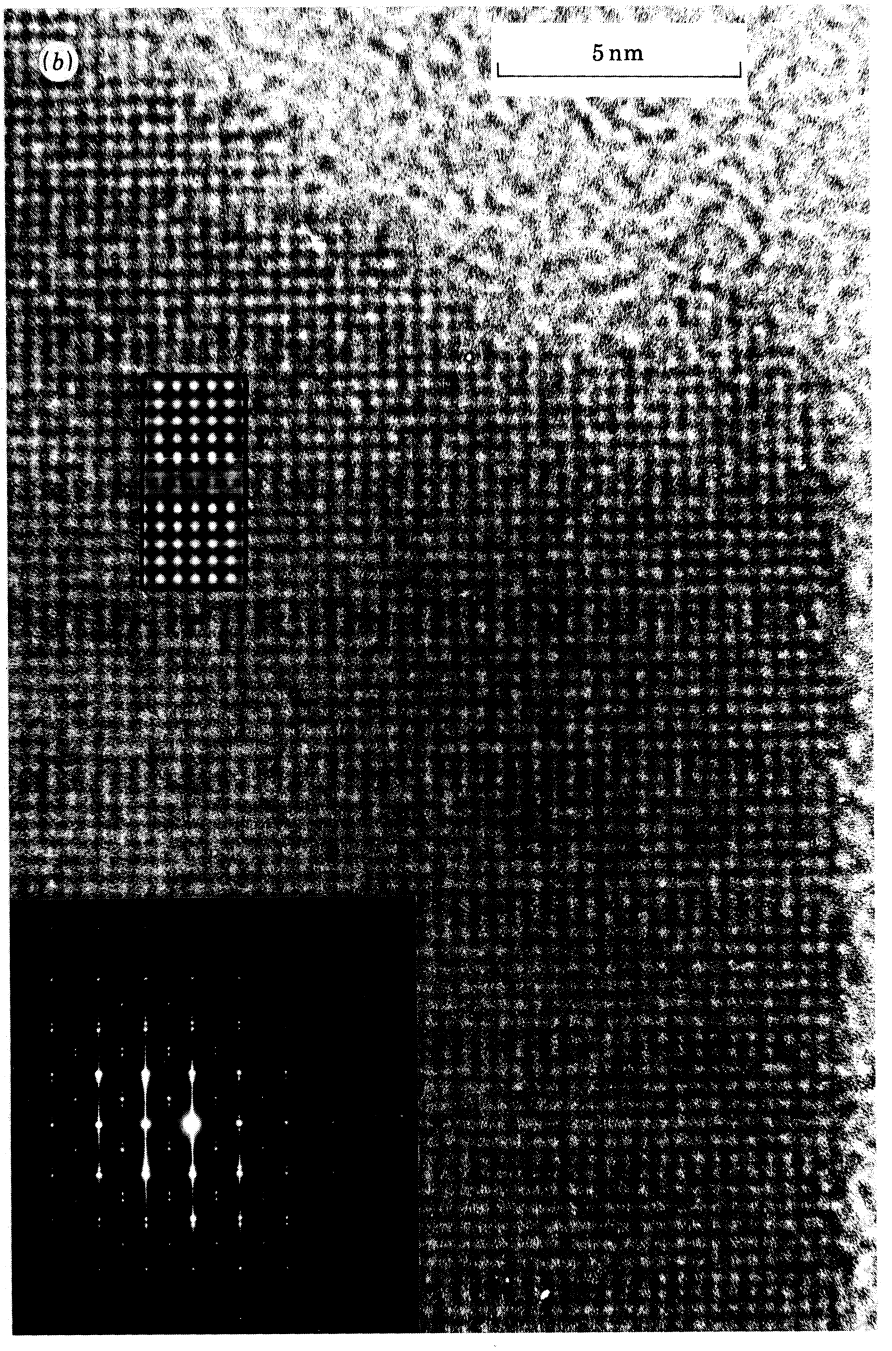

FIGURE 11 (*b*). For full description see opposite.

Downloaded from rspa.royalsocietypublishing.org on 17 June 2009

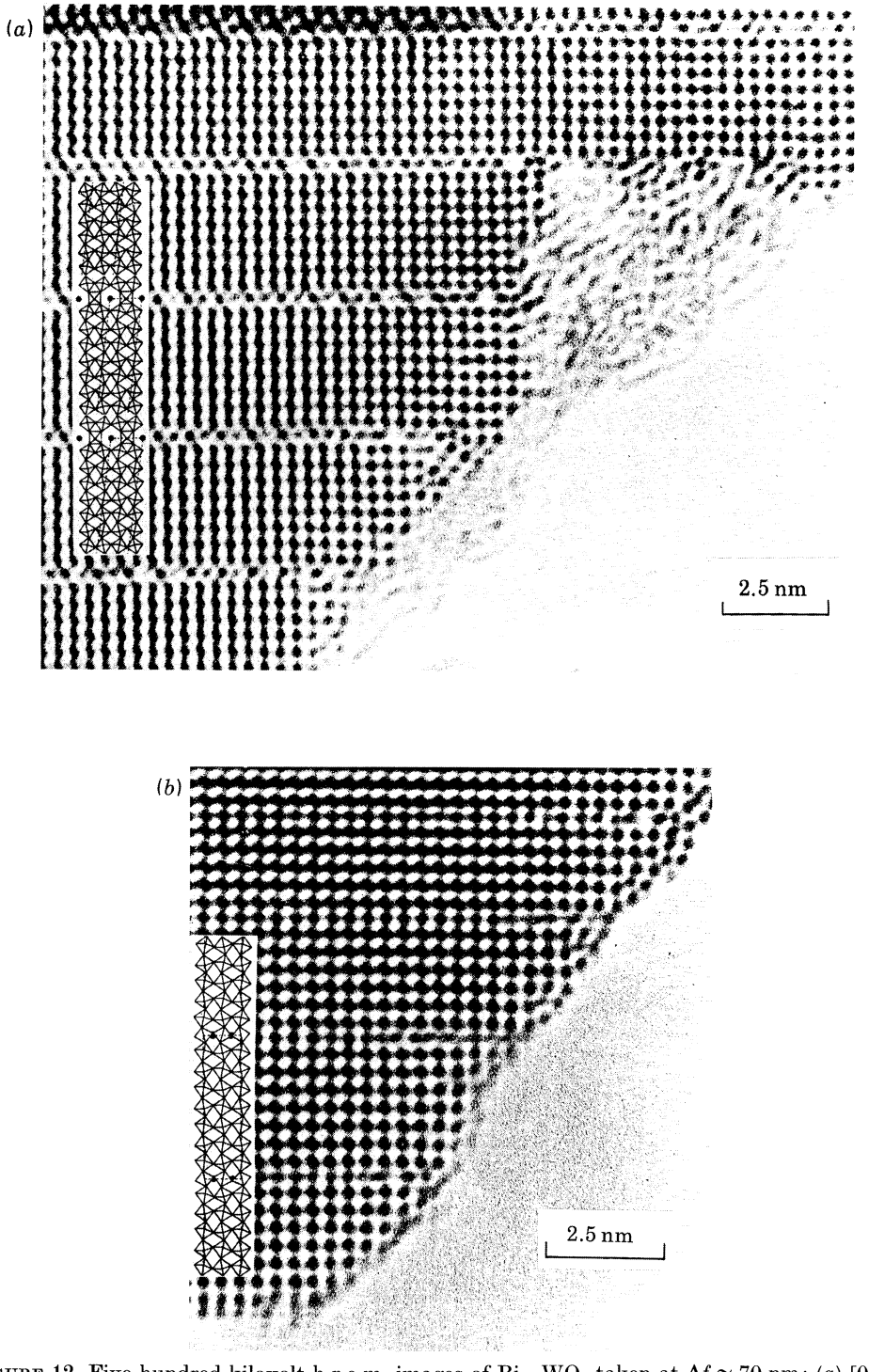

FIGURE 12. Five hundred kilovolt h.r.e.m. images of $Bi_{0.1}WO_3$ taken at $\Delta f \approx 70$ nm: (*a*) [001] projection showing apparently empty, or under occupied tunnels; (*b*) [010] projection. The corresponding structural models are also shown.

Downloaded from rspa.royalsocietypublishing.org on 17 June 2009

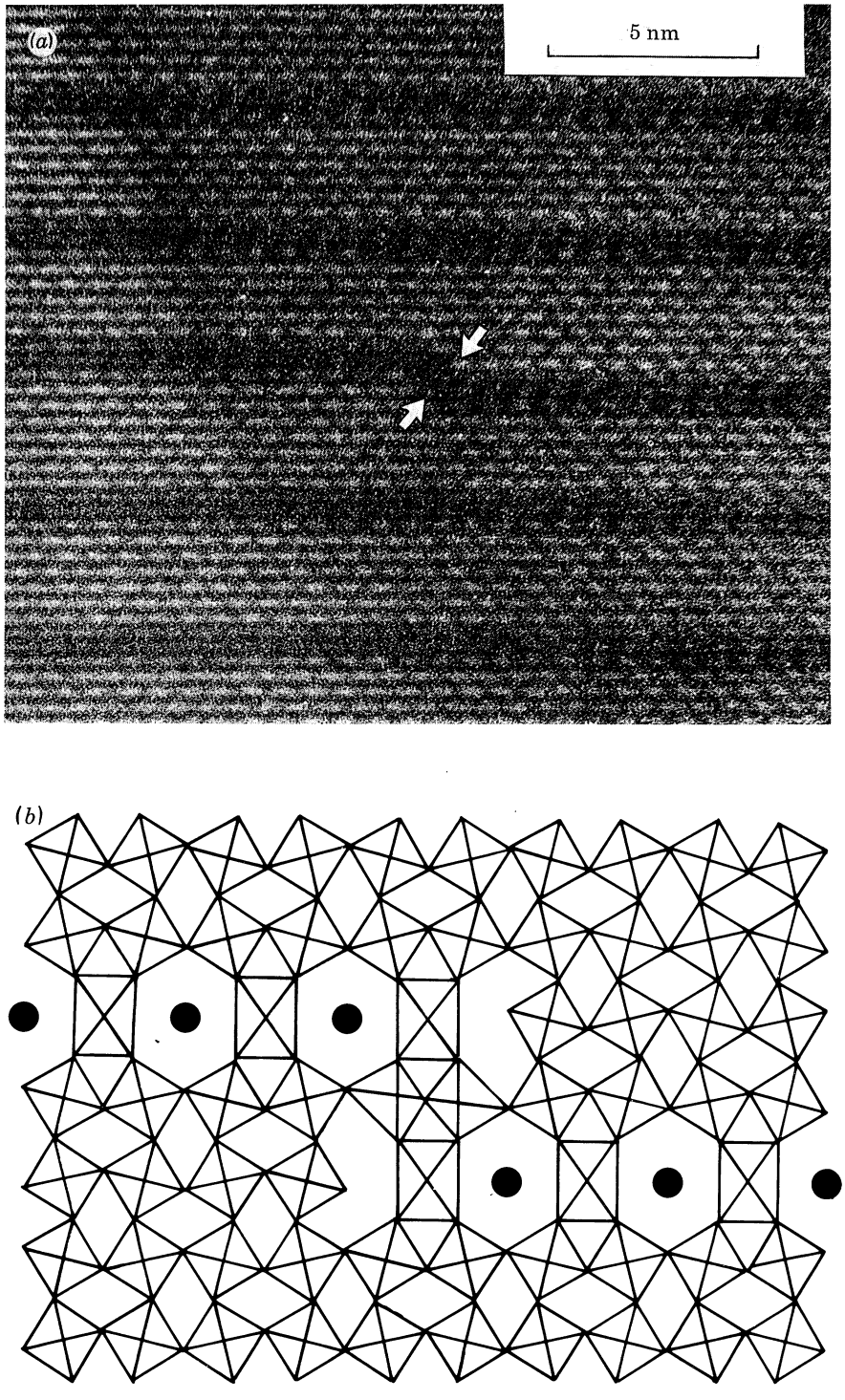

FIGURE 13. (*a*) Step in a h.t.b. strip (indicated) within a thick (over 10 nm) crystal of $Bi_{0.1}WO_3$ (nominal). (*b*) Schematic illustration of the local environment by using $Mo_{17}O_{47}$ as a model.

Downloaded from rspa.royalsocietypublishing.org on 17 June 2009

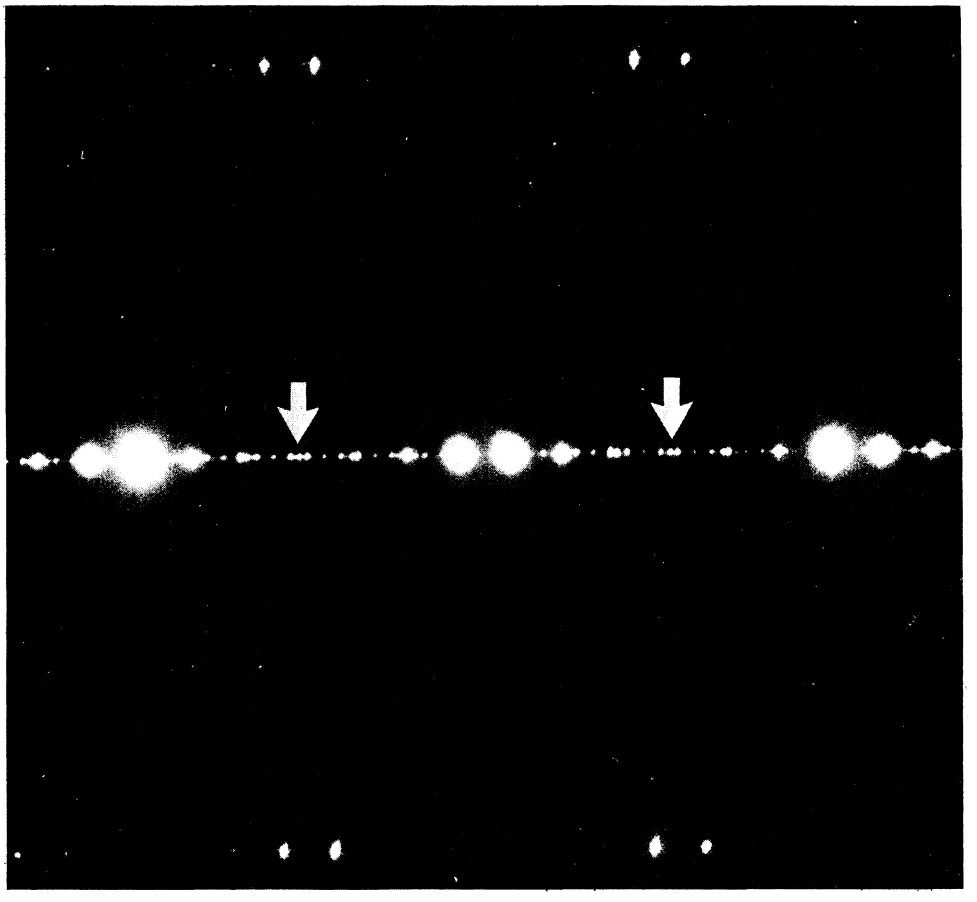

FIGURE 14. Satellites accompanying the superlattice spots in a crystal of $Bi_{0.1}WO_3$ (nominal). The overall periodicity of the satellite spot spacing corresponds to *ca.* 16 nm. The pattern corresponds to [011] projection.

Downloaded from rspa.royalsocietypublishing.org on 17 June 2009

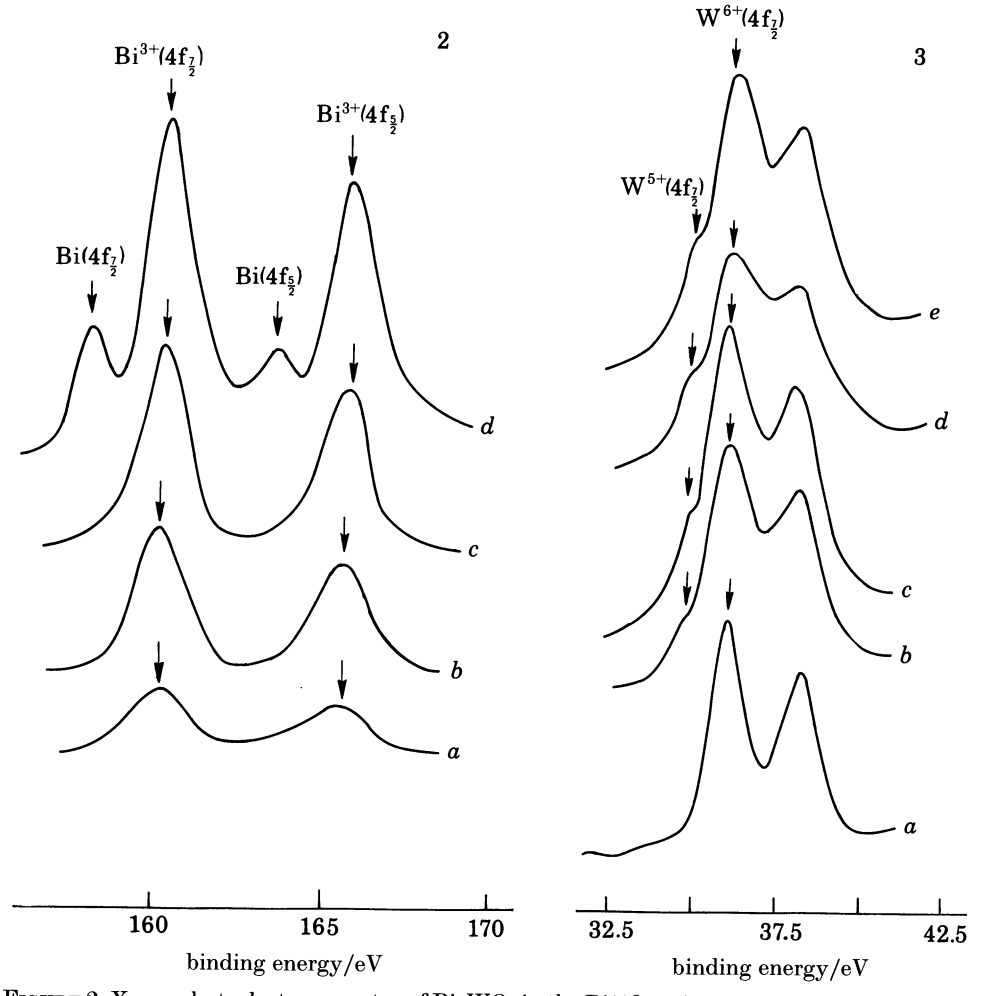

FIGURE 2. X-ray photoelectron spectra of Bi_xWO_3 in the Bi(4f) region: (*a*) $x = 0.01$; (*b*) $x = 0.05$; (*c*) $x = 0.10$ and (*d*) $x = 0.20$. Arrows indicate peak positions of Bi^{3+} and Bi^0. Metallic Bi^0 is present in the samples since all the bismuth is not incorporated in the tunnels of WO_3. Progressive increase of Bi^{3+} with increase in x can be seen.

FIGURE 3. X-ray photoelectron spectra of Bi_xWO_3 in the W(4f) region: (*a*) $x = 0.00$; (*b*) $x = 0.01$; (*c*) $x = 0.05$; (*d*) $x = 0.10$ and (*e*) $x = 0.20$. Arrows indicate $4f_{\frac{7}{2}}$ peaks of W^{5+} and W^{6+}.

Electron diffraction patterns of this specimen showed a superstructure of the basic ReO_3 structure, involving an approximate doubling of the pseudocubic a_c axis in all the three directions (figure 5, plate 2). It is possible that this phase corresponds to the perovskite-like bronze structure reported by Parmentier & Gleitzer (1975). Some crystals of the $x = 0.01$ sample occasionally showed diffraction patterns (see figure 5*d*) similar to the patterns of the samples with $x \geqslant 0.02$. X-ray powder diffraction patterns of the samples with $x \geqslant 0.02$ were complex and markedly different from the pattern exhibited by the $x = 0.01$ sample. Their analysis could only be achieved through a study of the electron diffraction patterns.

Downloaded from rspa.royalsocietypublishing.org on 17 June 2009

Crystals from all samples with $x \geqslant 0.02$ regularly showed electron diffraction patterns characteristic of an i.t.b. phase. With the high-tilt side-entry stage, it was possible to establish that almost identical reciprocal lattice sections exhibiting a one-dimensional superlattice were obtained down two mutually perpendicular directions within the plane of the WO_3 slabs (figure 6*a*, *b*, plate 3). The average superlattice periodicity varied from *ca.* 2.3 nm in $Bi_{0.2}WO_3$ to approximately 4.5 nm in $Bi_{0.02}WO_3$, but wide variations were obtained from different crystals in each sample. When viewed down a third principal axis, perpendicular to the slabs, the reciprocal lattice sections of all samples were identical and resembled the [001] projection of WO_3 (figure 6*c*). Apart from fragments that were clearly metallic bismuth contaminants, the bismuth content of the samples $x = 0.02$, 0.05 and 0.1 was impossible to determine accurately by X-ray emission analysis. With the sample of nominal composition $Bi_{0.2}WO_3$, however, a bismuth signal could be detected and qualitatively estimated in the crystals used for h.r.e.m. studies (figure 7, plate 4). By using previously characterized samples of Bi_2WO_6 and $Bi_2W_2O_9$ as standards, both of which are beam-stable under normal conditions (Jefferson 1982), the average composition of the i.t.b.-like crystals in this specimen was assessed as $Bi_{0.07}WO_3$, with a mean variation of some 25%, over a sample of approximately twenty crystals.

Analysis of all the samples, however, became possible by means of X-ray photoelectron spectra (X.p.s.). The spectra (figures 2 and 3) established the presence of bismuth in all the samples ($x \geqslant 0.01$) and also enabled analysis of the composition based on the W^{5+}/W^{6+} intensity ratios in the 4f spectra. The actual value of x in Bi_xWO_3 so determined for the nominal compositions with $x = 0.01$, 0.02, 0.05, 0.10 and 0.20 was 0.01, 0.02, 0.03, 0.05 and 0.06 respectively. Some of the bismuth is obviously not used in the reaction, as indeed is shown by X.p.s. (figure 2). The uncertainties in x values determined by X.p.s. would be around 15%, but it is gratifying that the actual value of x in $Bi_{0.2}WO_3$ (nominal) by this method agrees so well with that obtained from X-ray emission analysis in the microscope. For convenience, we shall use the nominal compositions throughout this paper.

By making use of the electron diffraction data, especially the supercell spots, we have analysed the rather complex X-ray diffraction patterns (figure 8) of Bi_xWO_3 samples with $x \geqslant 0.02$. The results are presented in table 1, where we have also given the values of x obtained from X-ray photoelectron spectroscopy. X-ray patterns of the samples with $x = 0.1$ and 0.2 appear to be due to mixtures of two predominant phases.

Ultrastructural studies of i.t.b. by h.r.e.m.

Typical h.r.e.m. images recorded at 200 kV from a sample of $Bi_{0.1}WO_3$ nominal composition are shown in figure 9, plate 5. The electron beam direction in each case is that of figure 6*a*. Disordered intergrowths of the type shown in figure 4*a* were obtained most frequently, but the minimum overall periodicity observed was generally not less than 1.9 nm. Well ordered crystals were comparatively rare. Figure 9*b* shows a micrograph of one such crystal taken at the defocus corresponding to highest obtainable resolution. Crystals also commonly showed a tendency to fragment at the edges (figure 9*c*), but no *in situ* conversion to WO_3 under conditions

Downloaded from rspa.royalsocietypublishing.org on 17 June 2009

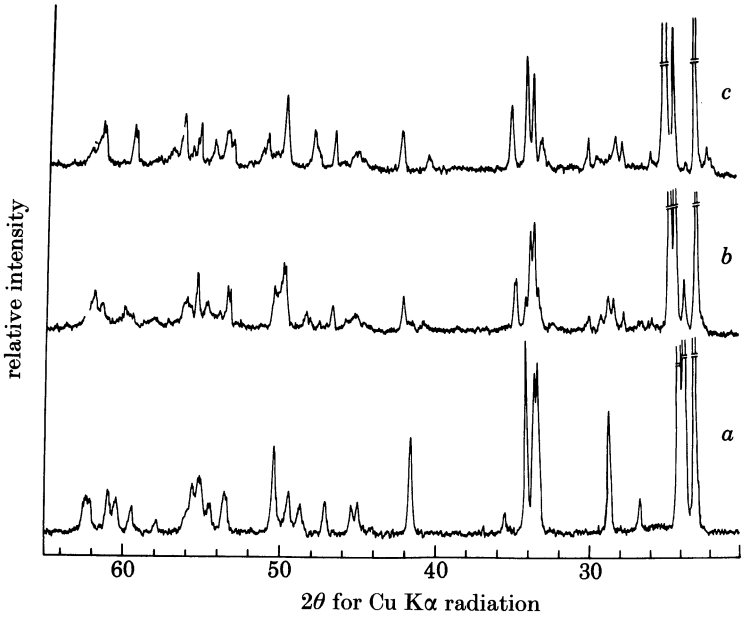

FIGURE 8. X-ray powder diffraction patterns of Bi_xWO_3: (*a*) $x = 0.01$; (*b*) $x = 0.05$ and (*c*) $x = 0.10$.

TABLE 1. UNIT CELL PARAMETERS OF Bi_xWO_3

x nominal	x actual[(a)]	n[(b)]	a/nm	b/nm	c/nm
0.02	0.016	13	5.10	0.735	0.390
0.05	0.028	12	4.88	0.735	0.390
0.10	0.05	8	3.22	0.735	0.391
		7	2.92	0.735	0.391
0.20	0.06	7	2.92	0.735	0.391
		6	2.51	0.735	0.391

(*a*) From X-ray photoelectron spectroscopy. (*b*) Number of supercell spots between two subcell spots along the a^* direction in the electron diffraction patterns.

of extremely high beam irradiation, as has been observed in h.r.e.m. images of $Bi_2W_2O_9$ (Bando *et al.* 1979), was noted.

H.r.e.m. evidence clearly indicated some form of i.t.b. structure. In particular, the regions of the crystals distinguished by their crossed 0.38 nm fringes of variable width were clearly slabs of WO_3, as expected. The structure of the intergrowth strip, however, was by no means clear. In particular, no well defined tunnels were observed, as for the known i.t.b. phases (Hussain & Kihlborg 1976; Ekstrom & Tilley 1980), the lack of clear detail in the strips being similar to that observed in Pb_xWO_3 at lower resolution (Ekstrom & Tilley 1978). As the existence of h.t.b. intergrowth strips was not conclusively established, image-matching studies were therefore made on three possible structural models, as shown in figure 10. The first of these (figure 10*a*) was essentially one involving intergrowth of perovskite

Downloaded from rspa.royalsocietypublishing.org on 17 June 2009

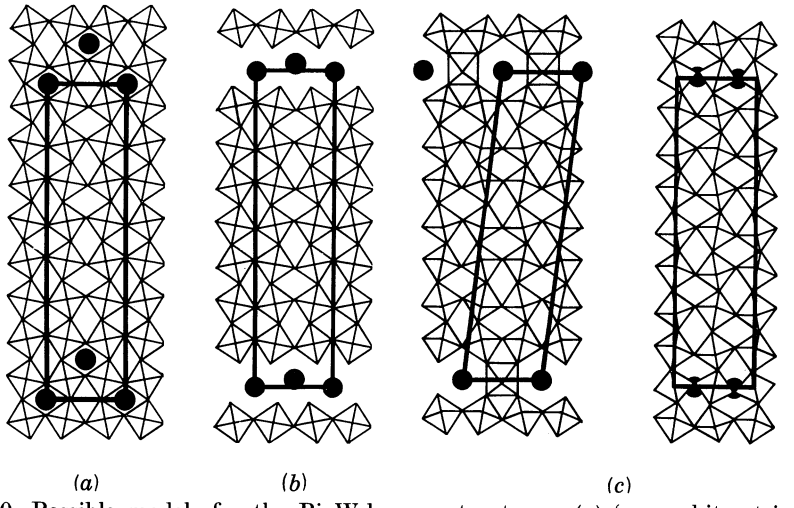

FIGURE 10. Possible models for the Bi–W-bronze structures: (*a*) 'perovskite strip' model; (*b*) 'isolated slab' model; (*c*) 'h.t.b.-strip' model, down both [001] and [010] projections.

strips, and did not correspond to observed images (at any values of crystal thickness) which require an excessive electron density along the intergrowth strips. The second model (figure 10*b*), involving isolated slabs of WO_3 separated by two-dimensional arrangements of bismuth atoms, gave reasonable agreement for thin crystals, but failed when the thickness exceeded 4.5 nm. Because of this partial agreement, and bearing in mind the closely similar electron scattering factors of tungsten and bismuth, a model was constructed by using h.t.b.-type intergrowth strips, but with completely filled channels (figure 10*c*). Although the projected charge density of this model was very similar to that of the previous one, the differences were sufficient to improve the fit at greater crystal thicknesses, and the overall stoichiometry of $Bi_{0.067}WO_3$ required was in good agreement with that observed experimentally for the nominal $Bi_{0.2}WO_3$ sample. The quality of the matching between observed and experimental images can be judged from figure 11*a*, plate 6, and 11*b*, plate 7, corresponding to the two directions of projection perpendicular to the superlattice axis. In particular, the way in which the model simulates apparently empty 'tunnels' at a crystal thickness of 6.0 nm in the projection of figure 11*a* is quite revealing, and suggests that in previous studies on other systems, lower than actual tunnel occupancies might have been assigned unless the crystals used for imaging were especially thin.

To confirm the structural model, 500 kV h.r.e.m. images were taken, trial simulations showing that at this level of resolution, it should be possible to distinguish between bismuth atoms within the tunnels and the tungsten atoms in the octahedra surrounding them. The results are indicated in figure 12, plate 8, for both projections, and with model structures inset. In the projection down the tunnel axis, a variation in the intensity of the dark dots within the intergrowth strips is noticeable. This phenomenon, which becomes more apparent upon prolonged exposure to the electron beam, appeared to be the beam-induced ejection of bismuth atoms from the tunnels in the very thin regions of the crystals.

Downloaded from rspa.royalsocietypublishing.org on 17 June 2009

It also provided a useful aid to characterizing conclusively the tunnel-like nature of the intergrowth strips. In the projection perpendicular to the tunnels, where the crystal fragments were extremely thin (figure 12*b*) a slight displacement of bismuth atoms within the tunnels might be inferred from the observed perturbations in the positions of the corresponding dark dots. In view of the demonstrated mobility of bismuth under 500 keV irradiation, however, such conclusions would have to be extremely speculative.

The structure derived for the Bi_xWO_3 phases fits in well with the data on other i.t.b. structures, and it would seem probable that the Pb_xWO_3 series also possess this structure. The retention of h.t.b.-type intergrowth strips for $0.01 < x < 0.05$ is, however, in conflict with previous data (Parmentier & Gleitzer 1975), which suggested a perovskite-like bronze within this composition range. The thermodynamic stability of regular bismuth bronze structures described above must, however, be in doubt, if only because of their apparent inability to form completely ordered structures, even upon prolonged re-annealing at 1170 K. The observed data indicates that bismuth will readily enter the WO_3 structure at this temperature to form isolated h.t.b. strips, which invariably extend completely across the crystals concerned. However, there is virtually no evidence for the mobility of the h.t.b. strips once formed. Very occasionally, steps can be observed in the intergrowth strips, as shown in figure 13*a*, plate 9. These invariably involve displacement of the strip by two WO_3 octahedra, and the break in the lines of tunnels can be reconciled with the grossly distorted hexagonal rings of $Mo_{17}O_{47}$ (Kihlborg 1960), as shown in figure 13*b*. However, such features appear to be relatively immobile, even under prolonged electron beam heating. Complete characterization was, however, impossible owing to the non-occurrence of these features in thin regions.

One other aspect of the Bi_xWO_3 structure that is not evident from the h.r.e.m. images is the actual positioning of bismuth atoms in the tunnels. In the model employed for the image simulations these are sited along the tunnel axes, at a level exactly between the surrounding layers of tungsten atoms, as in the rubidium and caesium bronzes (Kihlborg 1979). In the image simulation shown in figure 11*b*, the fact that the calculated contrast along the tunnel regions is less than that actually observed suggests that the height of the bismuth atoms in the tunnels may not be correct. This is further emphasized by the h.r.e.m. image of figure 12*b*, where, if the proposed model is adhered to absolutely, a continuous dark fringe along the tunnel axis might be expected, especially in the thin regions of the crystals. A further complication arises over the centring of bismuth atoms along the tunnel axes. By virtue of its lone pair of electrons, bismuth is a relatively large atom ($r = 0.102$ nm), but its electron density is unlikely to be spherically symmetric, and some displacement towards the tunnel sides is therefore likely. No evidence for this is found in h.r.e.m. images, nor would such small displacements be resolved, but if such displacements do exist, then the possibility of their ordering cannot be discounted. Some evidence for this can be seen in the selected area electron diffraction patterns of well annealed crystals, such as the one shown in figure 14, plate 10. This shows that the superlattice spots themselves possess a satellite structure, with an overall structural periodicity of *ca.* 16 nm. This is not merely

Downloaded from rspa.royalsocietypublishing.org on 17 June 2009

due to an intergrowth of two bronzes with a different periodicity, which would affect all rows parallel to X^* (to use the nomenclature of Hussain & Kihlborg (1976)). Instead, only rows with $l = 2n$ are affected, which suggests a more subtle explanation, possibly involving lateral displacements of the cations within the hexagonal tunnels. No perceptible contrast effects due to these satellites are seen in the h.r.e.m. images; consequently these features must await some form of single-crystal diffraction analysis, if sufficiently large crystals can be obtained.

Several features of the bismuth intergrowth tungsten bronzes are noteworthy. (i) The maximum value of x in Bi_xWO_3 i.t.b. phases is *ca.* 0.10, just as in other i.t.bs. (ii) The h.t.b. strips are, however, always isolated, the width being limited to that of a single tunnel. This is in contrast to the behaviour of alkali metal i.t.b. phases where two-tunnel wide h.t.b. strips are most stable. (iii) Although i.t.b. phases with long-range order containing only one type of arangement of the h.t.b. strips with respect to the WO_3 slabs are not found, we have not infrequently observed recurrent ordered intergrowths extending up to 100 nm in several crystals. (iv) Presence of widely different periodicities in the same 'single' crystal is common, but we can assign unit cell dimensions based on diffraction patterns. Presence of a variety of periodicities (and hence compositions) in the same crystal has been noted earlier in other complex oxide phases. We could, in principle, consider such crystals as composed of solid solutions of different phases; since we can still assign unit cell dimensions, we can treat the single crystals as ones possessing considerable disorder. We cannot, however, stop wondering about the traditional definitions of terms such as 'a phase' and 'a unit cell'. Certainly, we have to make a distinction between ultramicrostructure as seen by h.r.e.m. and the average structure. Yet, it is not clear how extensive the repetitive order in the ultrastructure should be before it represents the average structure.

H.t.b. phase of bismuth

Having failed to observe h.t.b. strips larger than a tunnel wide in the i.t.b. phases prepared by the reaction of bismuth with WO_3 at high temperatures, we attempted to make the pure h.t.b. phase by reaction of bismuth with hexagonal WO_3 (Gerand *et al.* 1979) below 500 °C. Two nominal compositions of Bi_xWO_3 ($x = 0.1$ and 0.2) so prepared were blue in colour and gave X-ray diffraction patterns characteristic of the h.t.b. phase. Based on the W^{5+}/W^{6+} intensity ratio in the 4f bands, we find that the actual value of x in the 0.1 and 0.2 samples work out to be 0.016 and 0.022 respectively. It appears that it is extremely difficult to incorporate bismuth in the hexagonal tunnel even by starting with hexagonal WO_3. This explains why we have not been able to obtain an i.t.b. phase to give way to a h.t.b. (or i.t.b.) phase at high concentrations of bismuth, by analogy with alkali metal i.t.b. systems.

X-ray lattice dimensions of the $x = 0.1$ and 0.2 h.t.b. phases were both close to $a = 0.74$ and $c = 0.76$ nm. Electron diffraction patterns showed no evidence for the ordering of bismuth atoms in the hexagonal tunnels of WO_3. This observation, along with the fact that the X-ray patterns showed the samples to be monophasic, suggest that bismuth atoms are randomly distributed in this h.t.b. The h.t.b. phase seems to be stable only up to 870 K, transforming to the i.t.b. phase at higher temperatures. The h.t.b. phase of bismuth is apparently metastable with respect to the i.t.b. phase.

Downloaded from rspa.royalsocietypublishing.org on 17 June 2009

Properties of i.t.b. phases

Optical absorption spectra of the i.t.b. phases (figure 15) show a progressive blue shift of the interband absorption edge around 450 nm with increasing x, just as in sodium–tungsten bronzes (Dickens *et al.* 1968). There is a broad band starting from 500 nm and extending to the near infrared in all these bronzes. These features are undoubtedly due to the creation of W^{5+} by bismuth atoms. With increase in x, the W(5d) band gets progressively filled, shifting the interband transition edge around 450 nm to shorter wavelengths. Accordingly, magnetic susceptibility of Bi_xWO_3 shows the expected changes. Compositions with $x < 0.05$ are diamagnetic and those with $x > 0.05$ are paramagnetic; paramagnetism in the latter is temperature-independent, suggesting the presence of itinerant electrons.

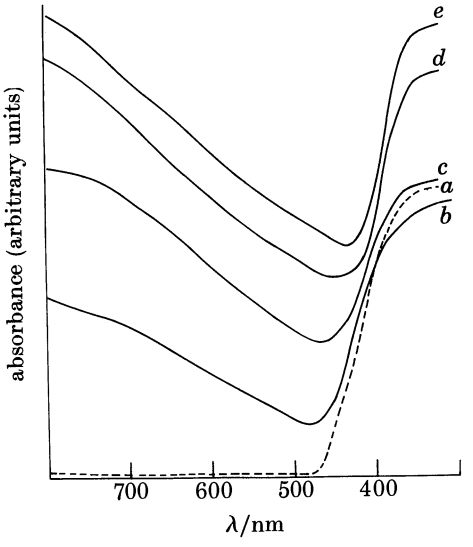

FIGURE 15. Reflectance spectra of Bi_xWO_3: (*a*) $x = 0.0$; (*b*) $x = 0.02$; (*c*) $x = 0.05$; (*d*) $x = 0.10$ and (*e*) $x = 0.20$.

Electron transport properties of the bronzes clearly show evidence for the itinerant nature of d electrons when $x > 0.05$. Electrical resistivity of Bi_xWO_3 decreases markedly with increase in x (figure 16), and when $x = 0.2$ (nominal) the resistivity at 300 K is barely 0.20 Ω cm. Seebeck coefficient data also reflect the changes in the electronic structure of the bismuth i.t.b. phases with increase in x (figure 17). The Seebeck coefficient (at 300 K) decreases sharply up to $x \approx 0.05$ (resistivity also drops markedly in this composition range). The absolute value of the Seebeck coefficient decreases with increase in temperature when $x < 0.05$, while the opposite holds when $x > 0.05$. It appears that the d electrons are localized when $x < 0.05$ and itinerant when $x > 0.05$. Based on the trends in transport properties reported here, we would expect Bi_xWO_3 to become metallic when x is *ca.* 0.08. Interestingly, this value of x is around one third the value in alkali metal bronzes, M_xWO_3, when they become metallic. Since bismuth can donate three electrons to WO_3, this is what we would expect.

Downloaded from rspa.royalsocietypublishing.org on 17 June 2009

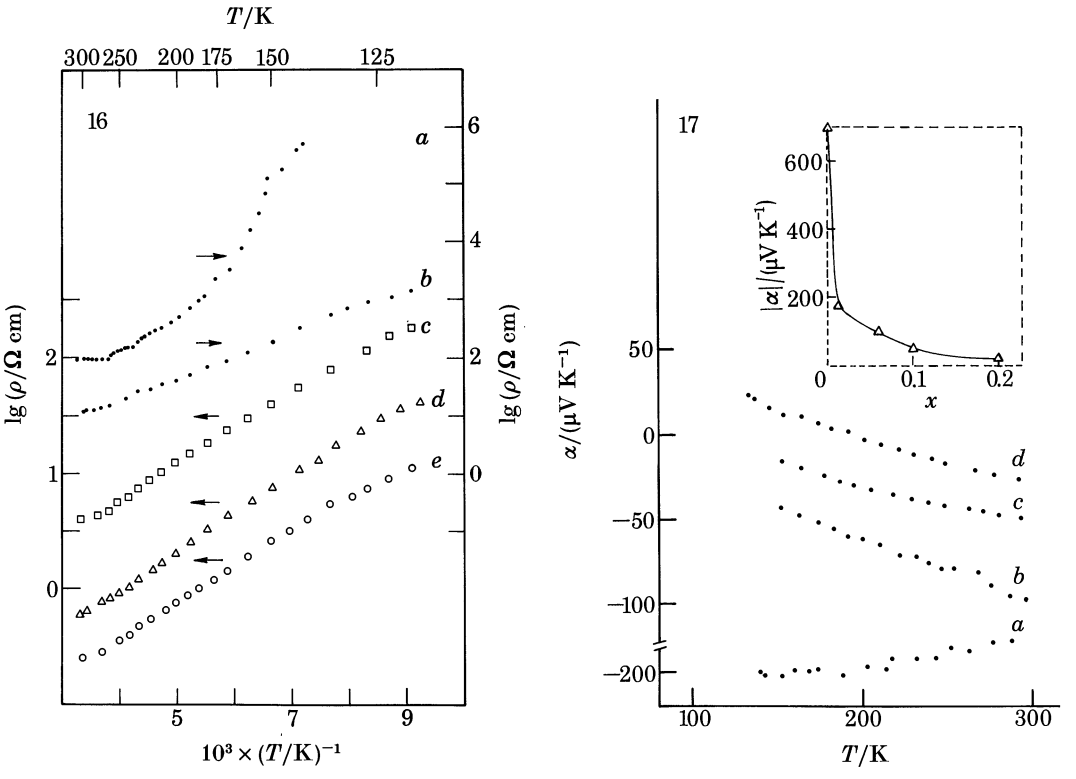

FIGURE 16. Variation of the electrical resistivity, p, of Bi_xWO_3 with temperature: (*a*) $x = 0.0$; (*b*) $x = 0.01$; (*c*) $x = 0.05$; (*d*) $x = 0.10$ and (*e*) $x = 0.20$. Resistivity data of WO_3 ($x = 0.0$) reflect the phase transitions exhibited by this oxide.

FIGURE 17. Variation of the Seebeck coefficient, α, of Bi_xWO_3 with temperature: (*a*) $x = 0.01$; (*b*) $x = 0.05$; (*c*) $x = 0.10$ and (*d*) $x = 0.20$. In the inset α at room temperature is plotted against x.

The authors thank Dr D. J. Smith of the High Resolution Electron Microscope, University of Cambridge, for his assistance in obtaining images on the 500 kV microscope. C.N.R.R. thanks the University Grants Commission of India for support of this research and the University of Cambridge for the Nehru Visiting Chair.

REFERENCES

Aurivillius, B. 1949 *Ark. Kemi* **1**, 463.
Bando, Y., Watanabe, A., Sekikawa, Y., Goto, M. & Horiuchi, S. 1979 *Acta Crystallogr.* A **35**, 142.
Dickens, P. G., Quillium, R. M. P. & Whittigham, M. S. 1968 *Mater. Res. Rull.* **3**, 941.
Ekstrom, T. & Tilley, R. J. D. 1978 *J. solid state Chem.* **24**, 209.
Ekstrom, T. & Tilley, R. J. D. 1980 *Chem. Scripta* **16**, 1.
Fejes, P. L. 1977 *Acta crystallogr.* A **33**, 109.
Gerand, B., Nowogrocki, G., Guenot, J. & Figlarz, M. 1979 *J. solid state Chem.* **29**, 429.
Goodman, P. & Moodie, A. F. 1974 *Acta crystallogr.* A **32**, 551.
Hussain, A. & Kihlborg, L. 1976 *Acta crystallogr.* A **32**, 551.
Hutchison, J. L., Anderson, J. S. & Rao, C. N. R. 1977 *Proc. R. Soc. Lond.* A **355**, 301.

Downloaded from rspa.royalsocietypublishing.org on 17 June 2009

Jefferson, D. A. 1982 *Phil. Trans. R. Soc. Lond.* A **305**, 535.
Jefferson, D. A., Gopalakrishnan, J. & Ramanan, A. 1982 *Mater. Res. Rull.* **17**, 269.
Kihlborg, L. 1960 *Acta chem. scand.* **14**, 1612.
Kihlborg, L. 1979 *Chem. Scripta* **14**, 187.
Lynch, D. F., Moodie, A. F. & O'Keefe, M. A. 1975 *Acta crystallogr.* A **31**, 300.
Parmentier, M. & Gleitzer, C. 1975 *C.r. hebd. Séanc. Acad. Sci. Paris* **281** C, 819.
Rao, C. N. R., Sarma, D. D., Vasudevan, S. & Hegde, M. S. 1979 *Proc. R. Soc. Lond.* A **367**, 239.
Smith, D. J., Camps, R. A., Cosslett, V. E., Freeman, L. A., Saxton, W. O., Nixon, W. C., Ahmed, H., Catto, C. J. D., Cleaver, J. R. A., Smith, K. C. A. & Timbs, A. E. 1982 *Ultramicroscopy* **9**, 203.

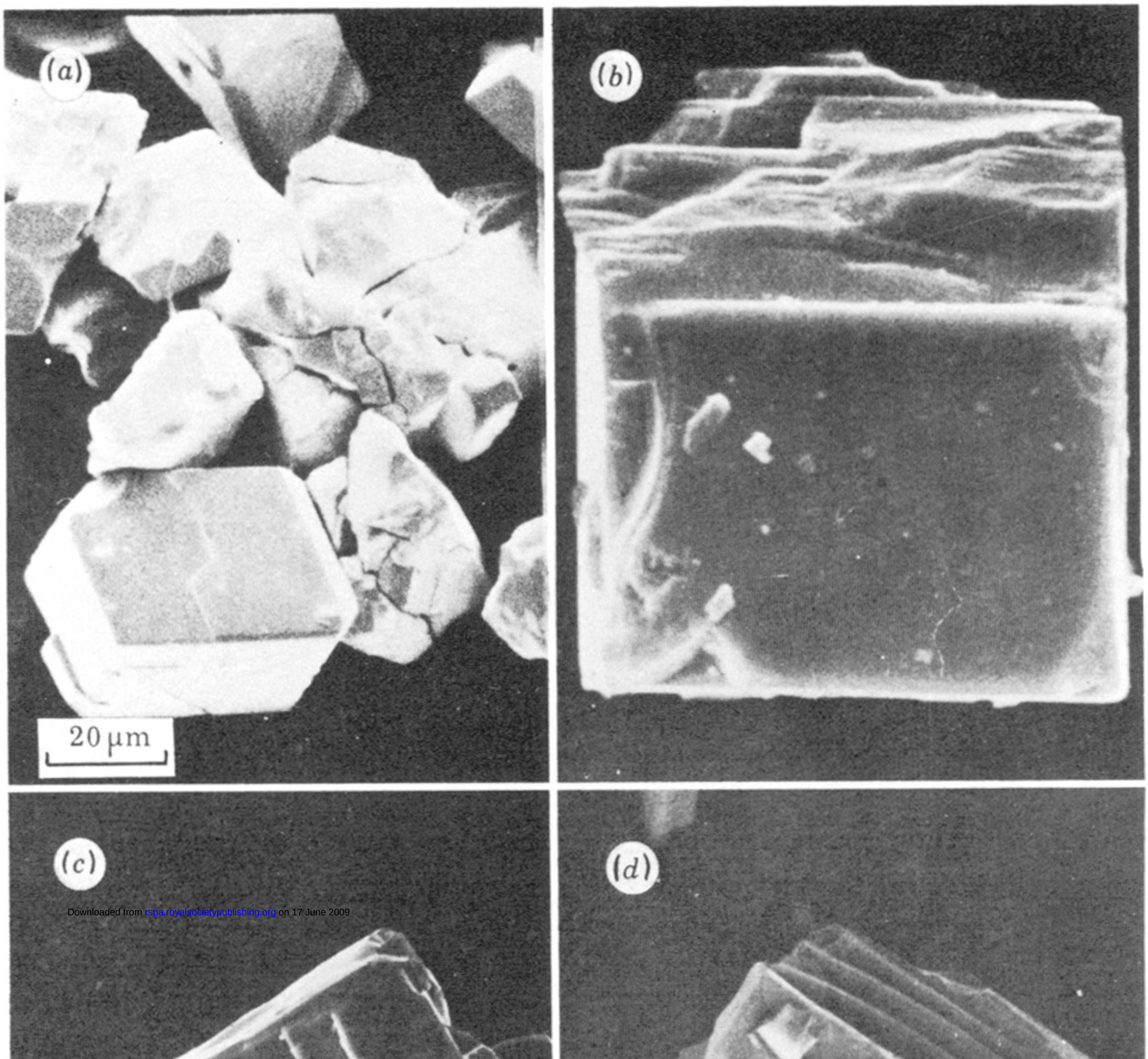

Downloaded from rspa.royalsocietypublishing.org on 17 June 2009

FIGURE 4. Scanning electron micrographs of Bi_xWO_3: (*a*) $x = 0.01$; (*b*) and (*c*) $x = 0.05$ and (*d*) $x = 0.10$. Magnifications are (*a*) $\times 2000$, (*b*) $\times 2000$, (*c*) $\times 1000$ and (*d*) $\times 5000$.

Downloaded from rspa.royalsocietypublishing.org on 17 June 2009

FIGURE 5. Electron diffraction patterns of WO_3-like crystals of $Bi_{0.01}WO_3$. Electron beam parallel to $[0\bar{1}0]$ in (*a*), [001] in (*b*) and $[01\bar{1}]$ in (*c*). The pattern of a minor phase showing streaking along a^* is shown in (*d*).

Downloaded from rspa.royalsocietypublishing.org on 17 June 2009

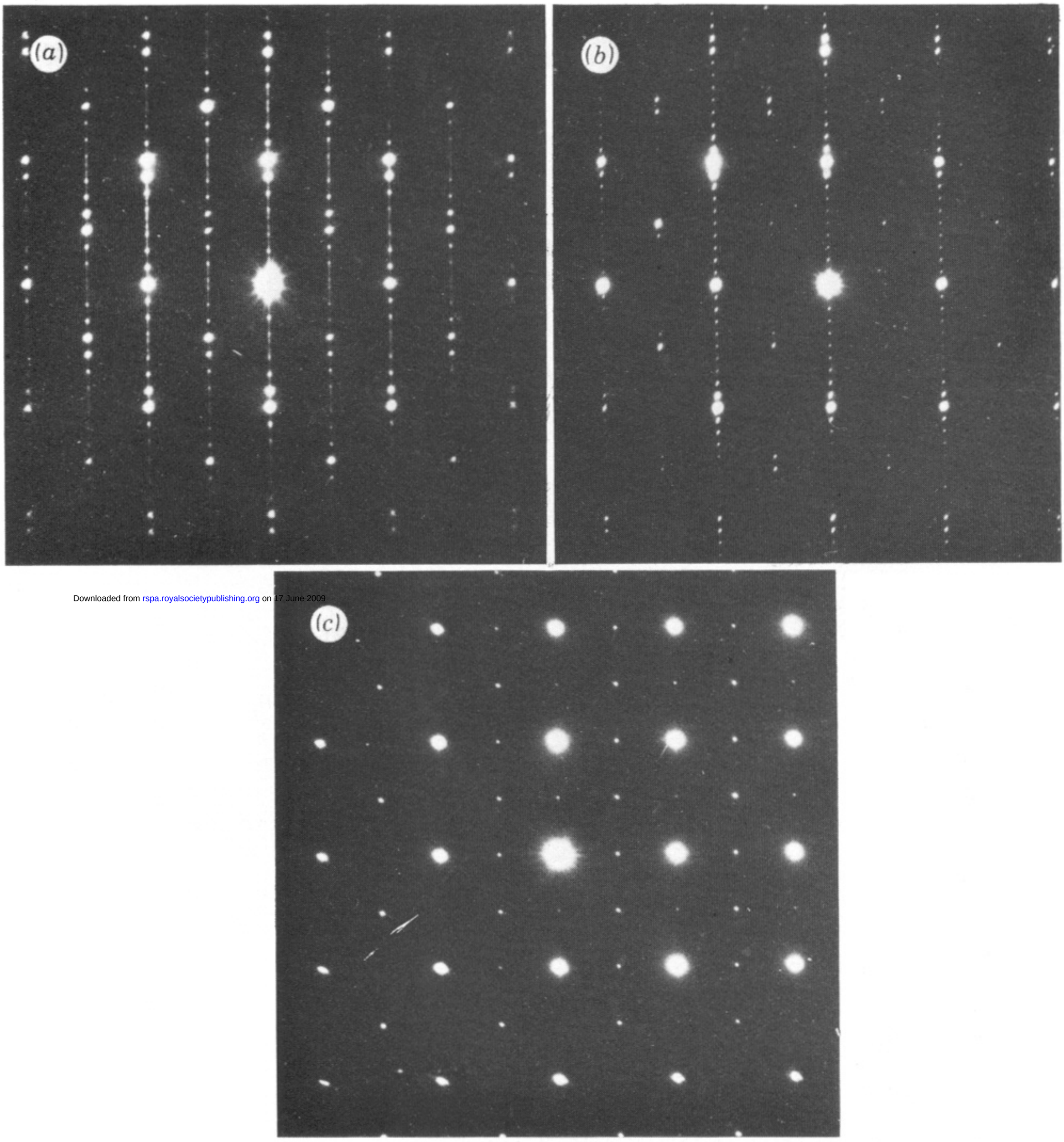

FIGURE 6. Typical s.a.e.d patterns of Bi–W-bronzes: (*a*) and (*b*) are principal sections showing the one-dimensional superlattice. These correspond to projection down [001] and [010] respectively, by the nomenclature of Hussain & Kihlborg (1976); (*c*) is the projection down the [100] axis.

Downloaded from rspa.royalsocietypublishing.org on 17 June 2009

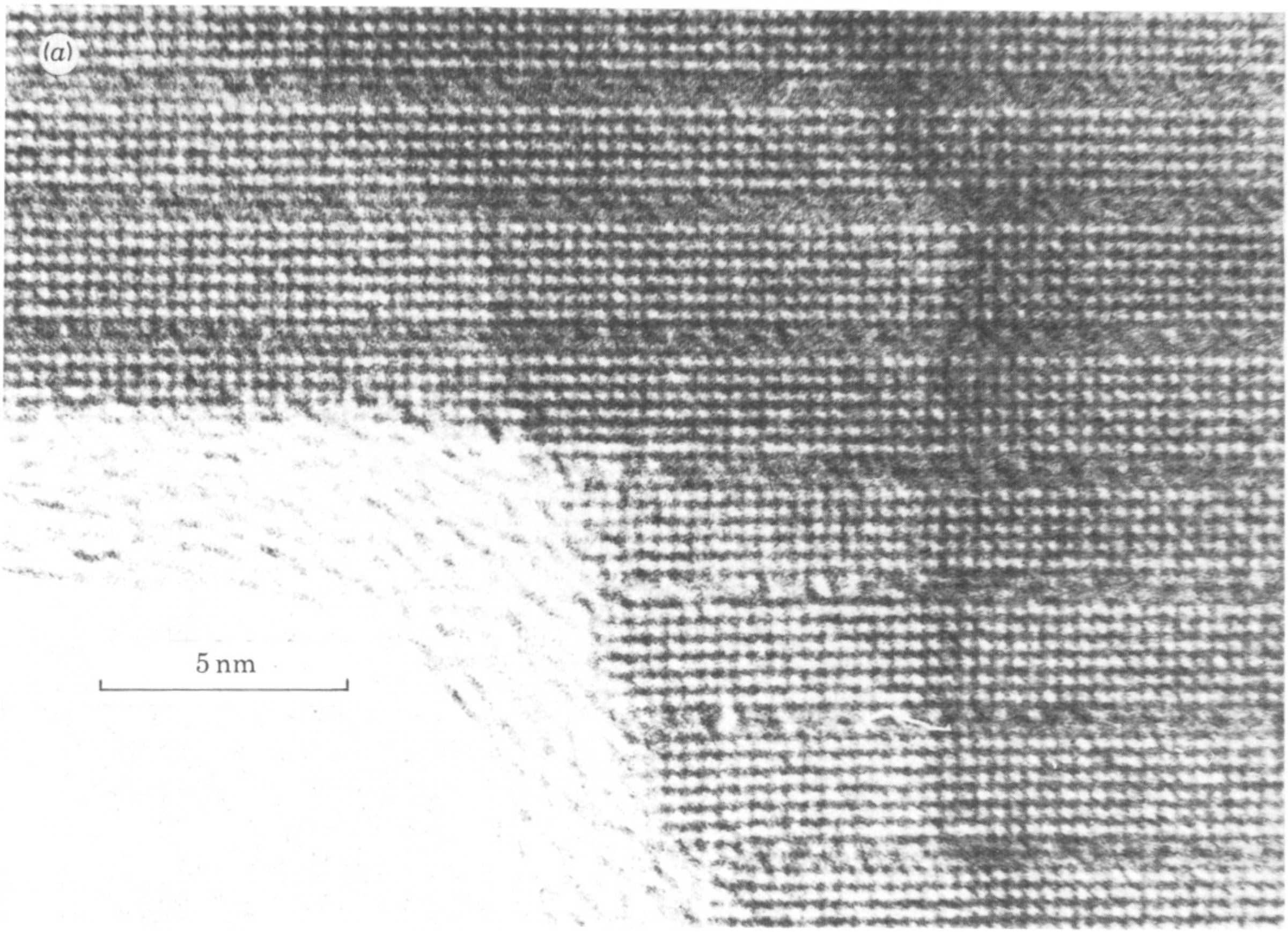

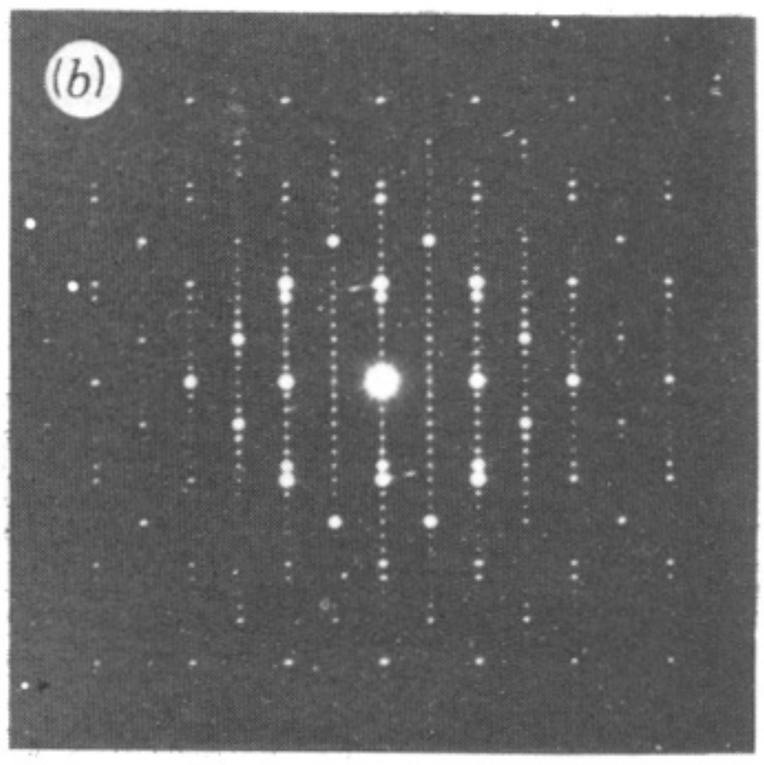

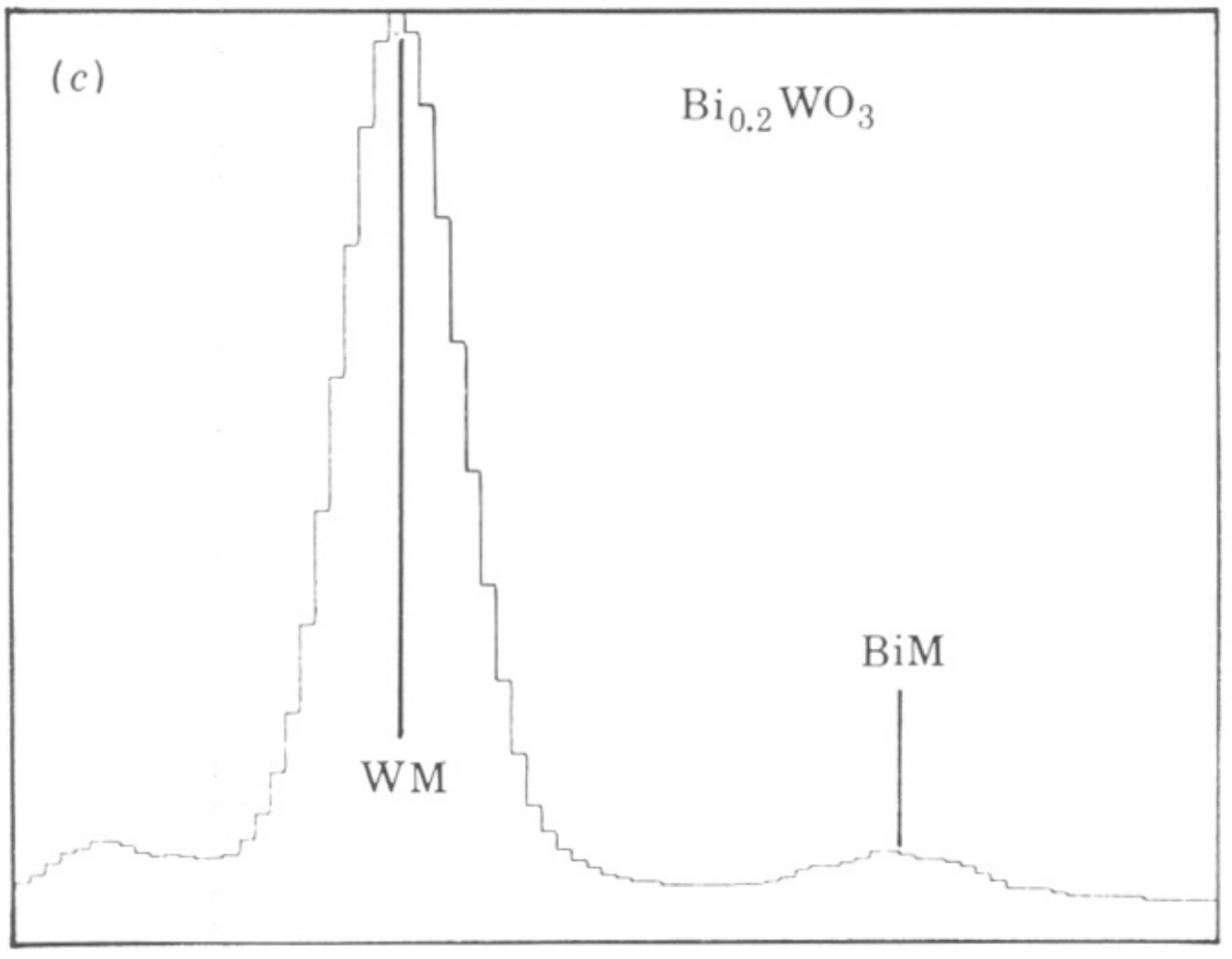

FIGURE 7. (*a*) h.r.e.m. (200 kV) image; (*b*) s.a.e.d. pattern and (*c*) part of the X-ray emission spectrum of a crystal of nominal composition of $Bi_{0.2}WO_3$. The image corresponds to the [001] projection.

Downloaded from rspa.royalsocietypublishing.org on 17 June 2009

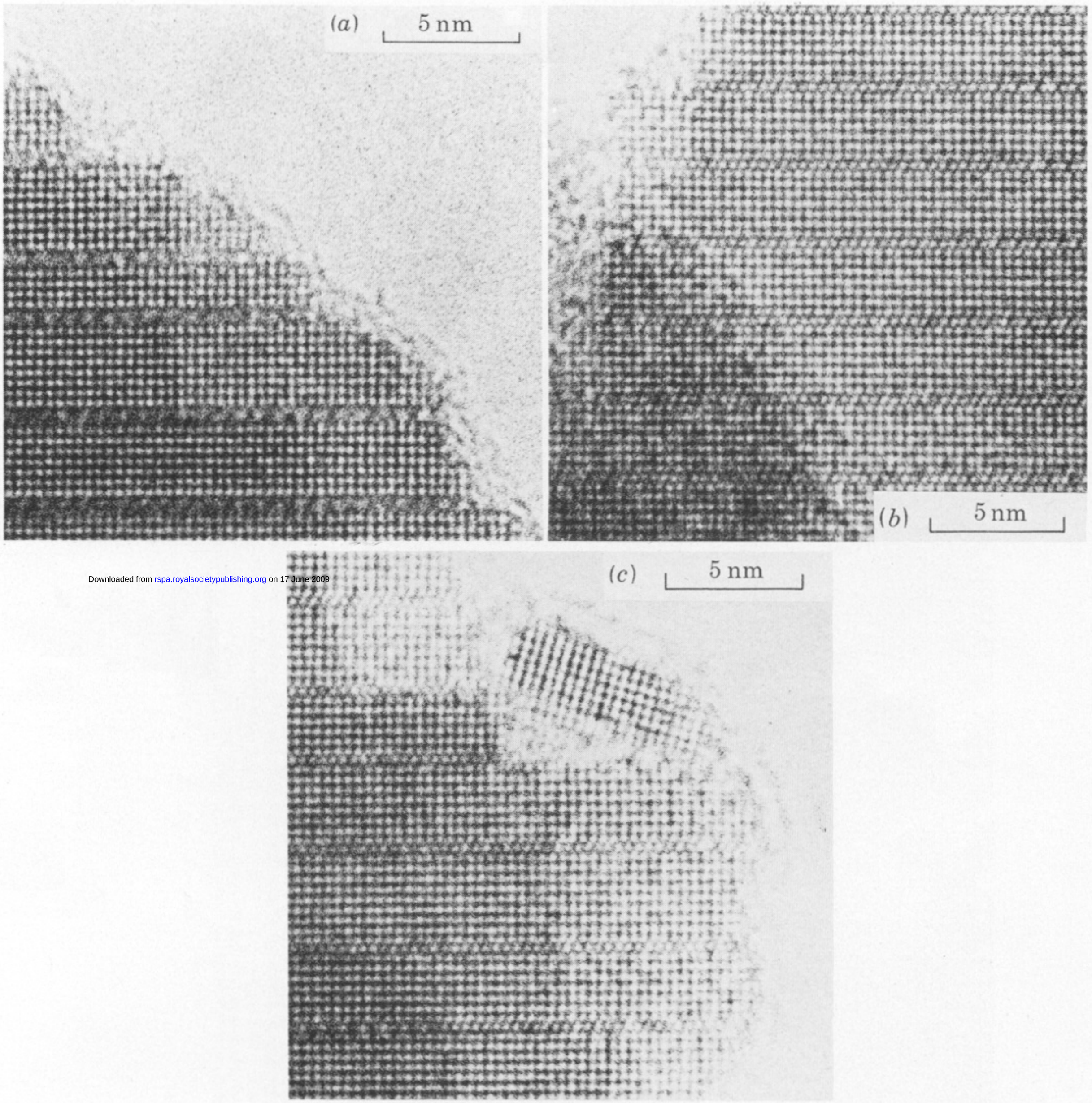

FIGURE 9. (*a*) H.r.e.m. image of a disordered intergrowth bronze of nominal composition $Bi_{0.1}WO_3$, $\Delta f \approx 150$ nm; (*b*) a more ordered crystal in the same sample, $\Delta f = 120$ nm; (*c*) crystal showing fragmentation at the edge, $\Delta f = 120$ nm. Axis of projection in each case is [001].

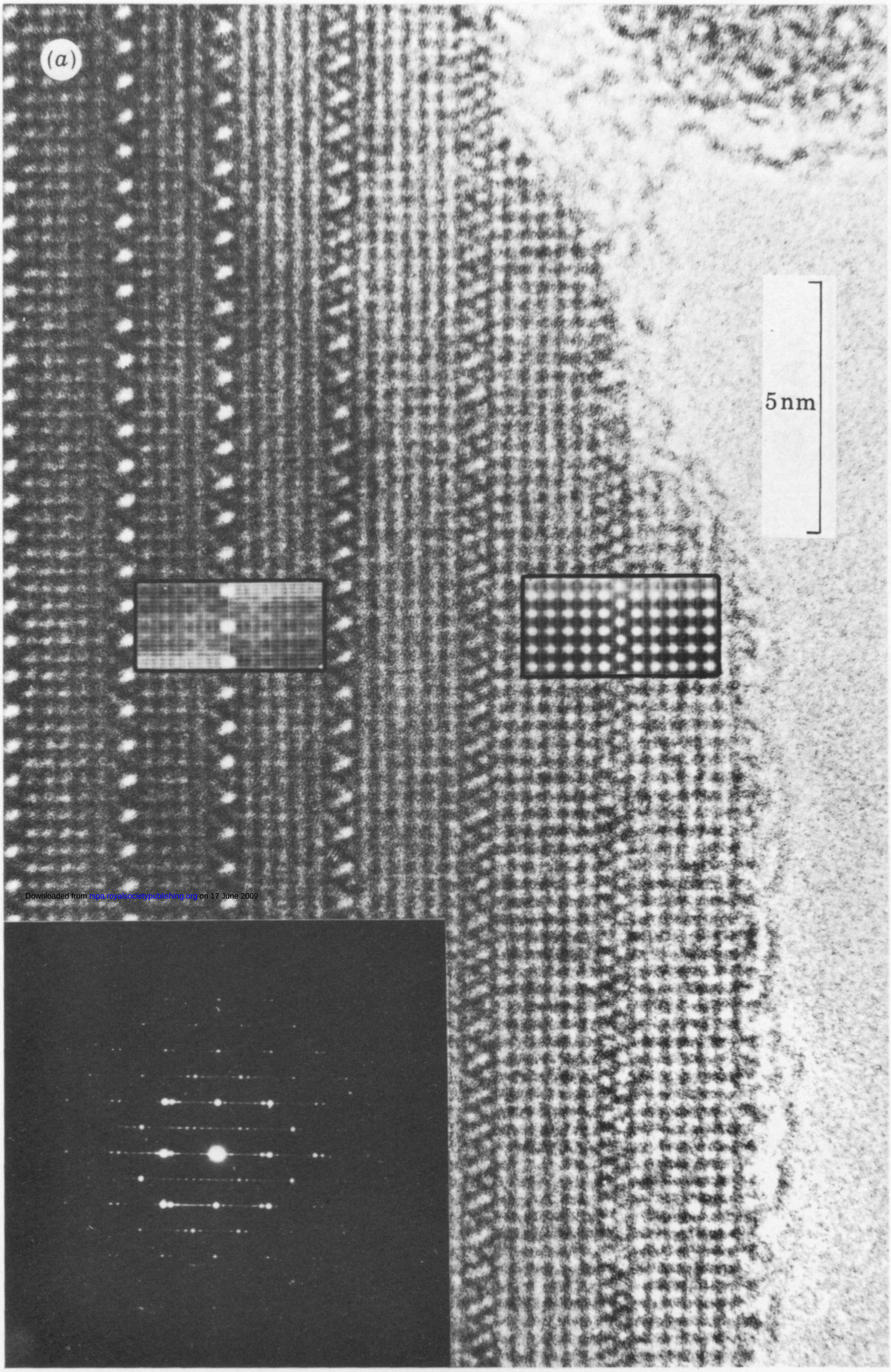

Downloaded from rspa.royalsocietypublishing.org on 17 June 2009

FIGURE 11. Image matching studies for the sample of nominal composition $Bi_{0.1}WO_3$. (*a*) [001] projection, simulations (inset) for crystal thickness of 3 nm (near edge) and 6 nm, $\Delta f = 120$ nm; (*b*) (opposite) [010] projection, simulation for crystal thickness of 4.5 nm and $\Delta f = 120$ nm. Completely filled tunnels in the simulations correspond to composition of $Bi_{0.067}WO_3$. The corresponding s.a.e.d. patterns are also shown.

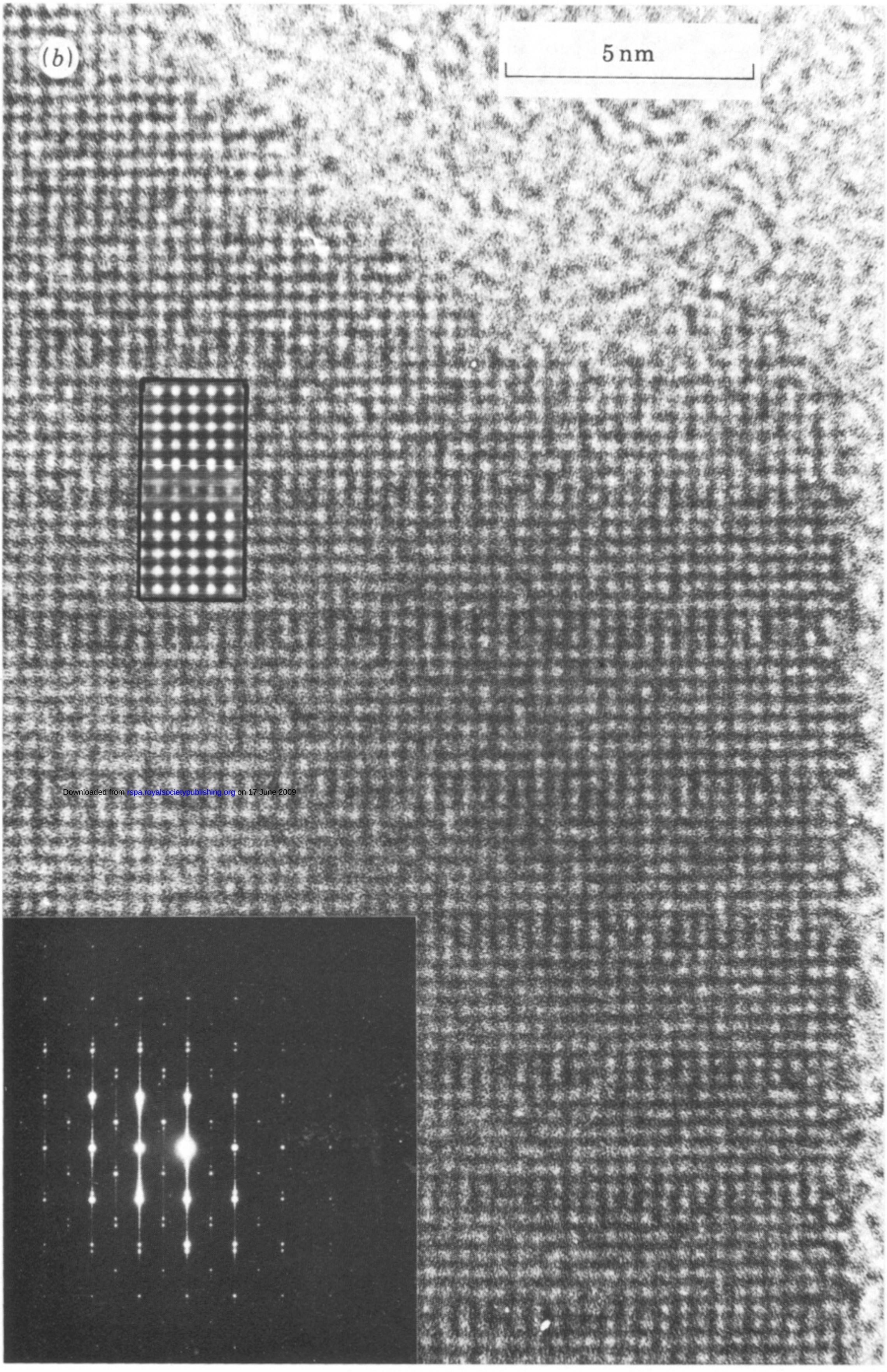

Downloaded from rspa.royalsocietypublishing.org on 17 June 2009

FIGURE 11 (*b*). For full description see opposite.

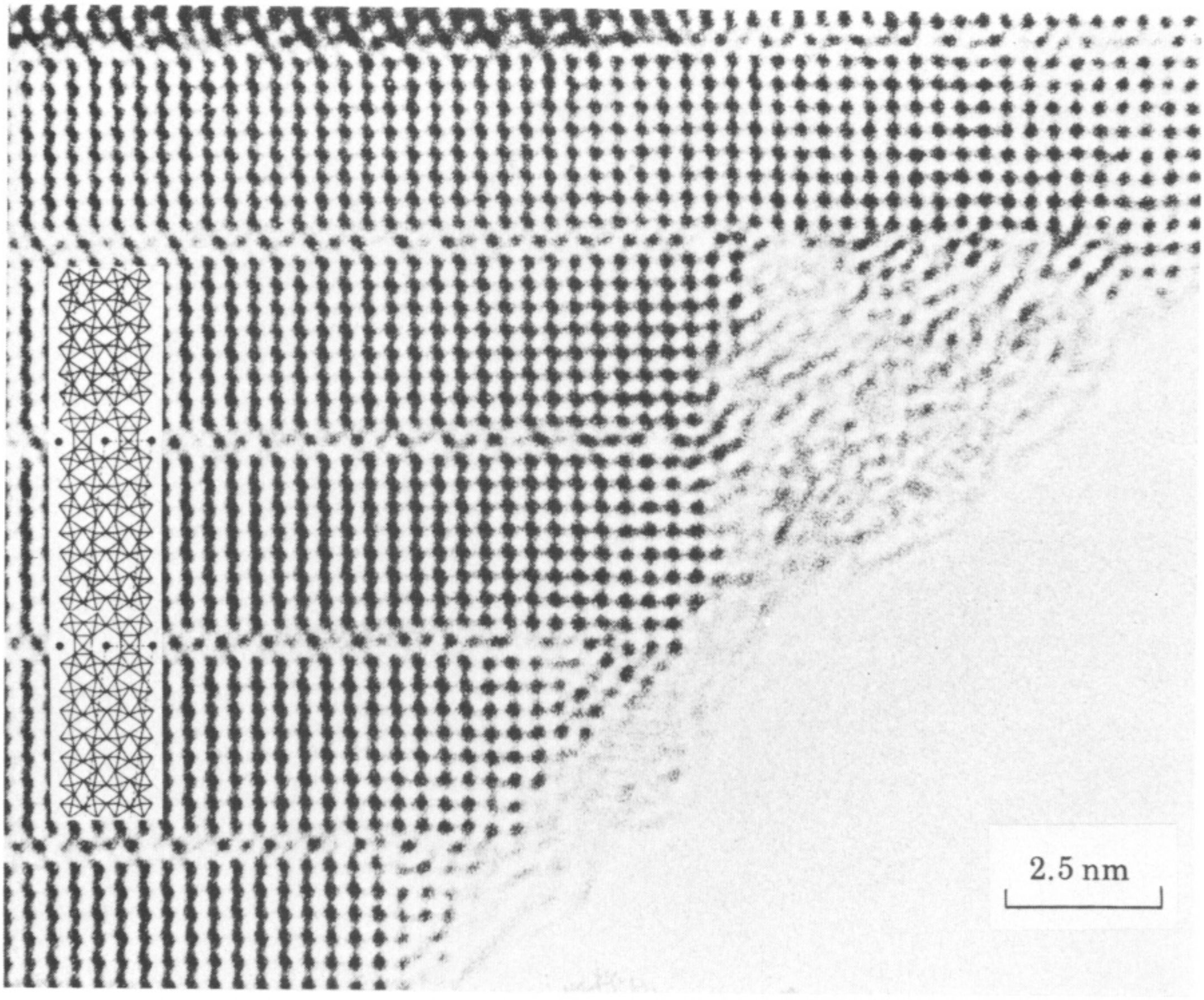

Downloaded from rspa.royalsocietypublishing.org on 17 June 2009

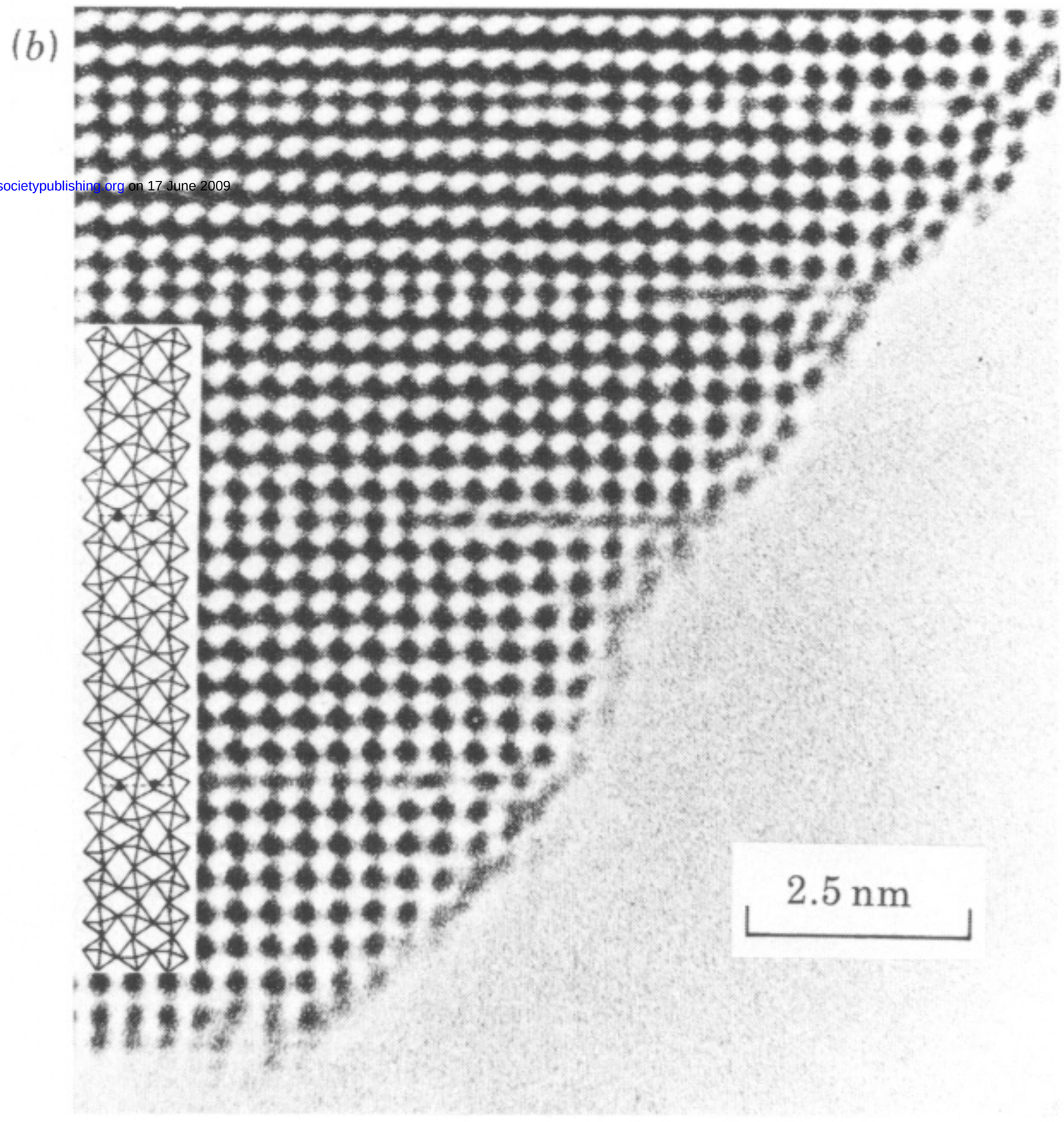

FIGURE 12. Five hundred kilovolt h.r.e.m. images of $Bi_{0.1}WO_3$ taken at $\Delta f \approx 70$ nm: (*a*) [001] projection showing apparently empty, or under occupied tunnels; (*b*) [010] projection. The corresponding structural models are also shown.

Downloaded from rsta.royalsocietypublishing.org on 17 June 2009

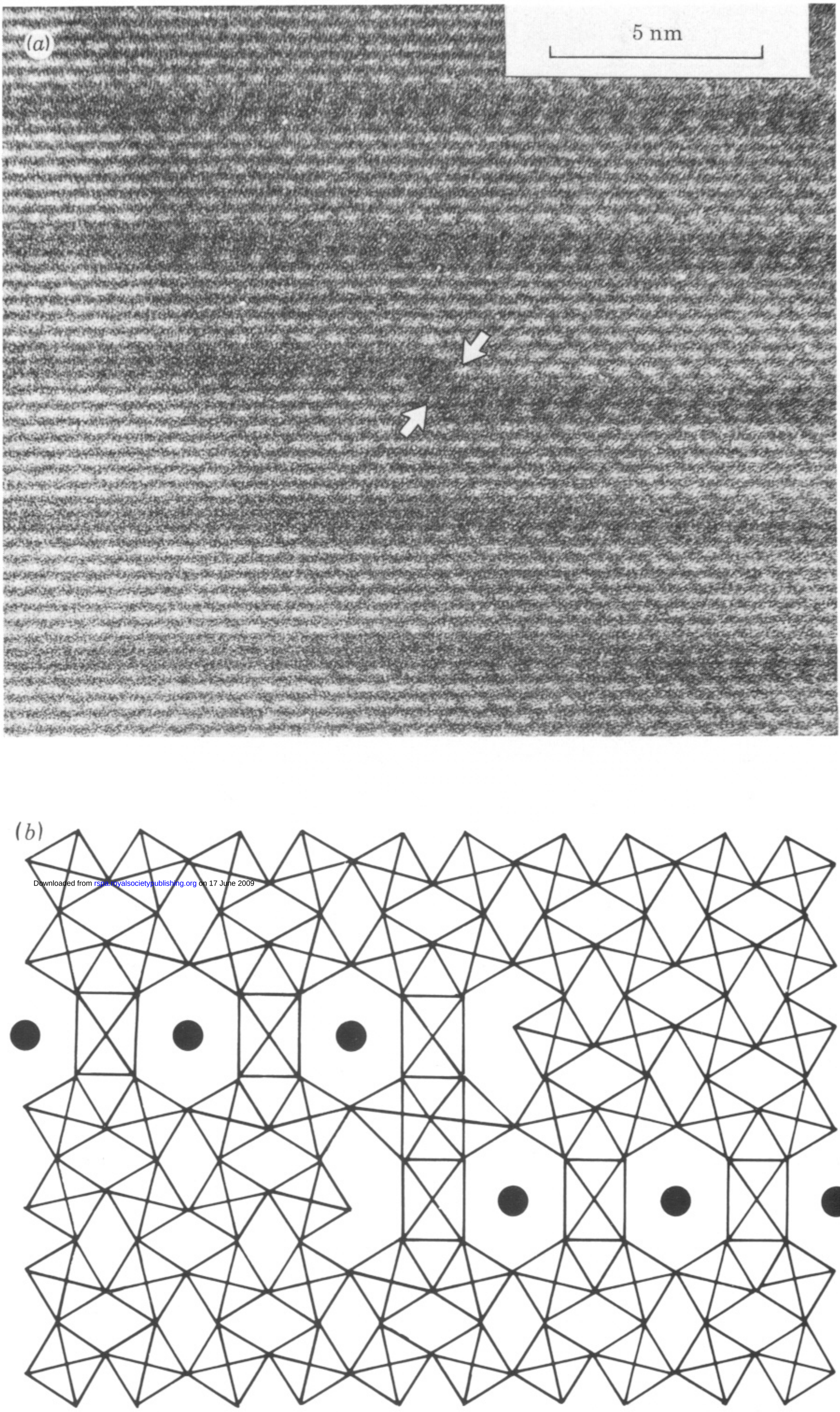

FIGURE 13. (*a*) Step in a h.t.b. strip (indicated) within a thick (over 10 nm) crystal of $Bi_{0.1}WO_3$ (nominal). (*b*) Schematic illustration of the local environment by using $Mo_{17}O_{47}$ as a model.

Downloaded from rspa.royalsocietypublishing.org on 17 June 2009

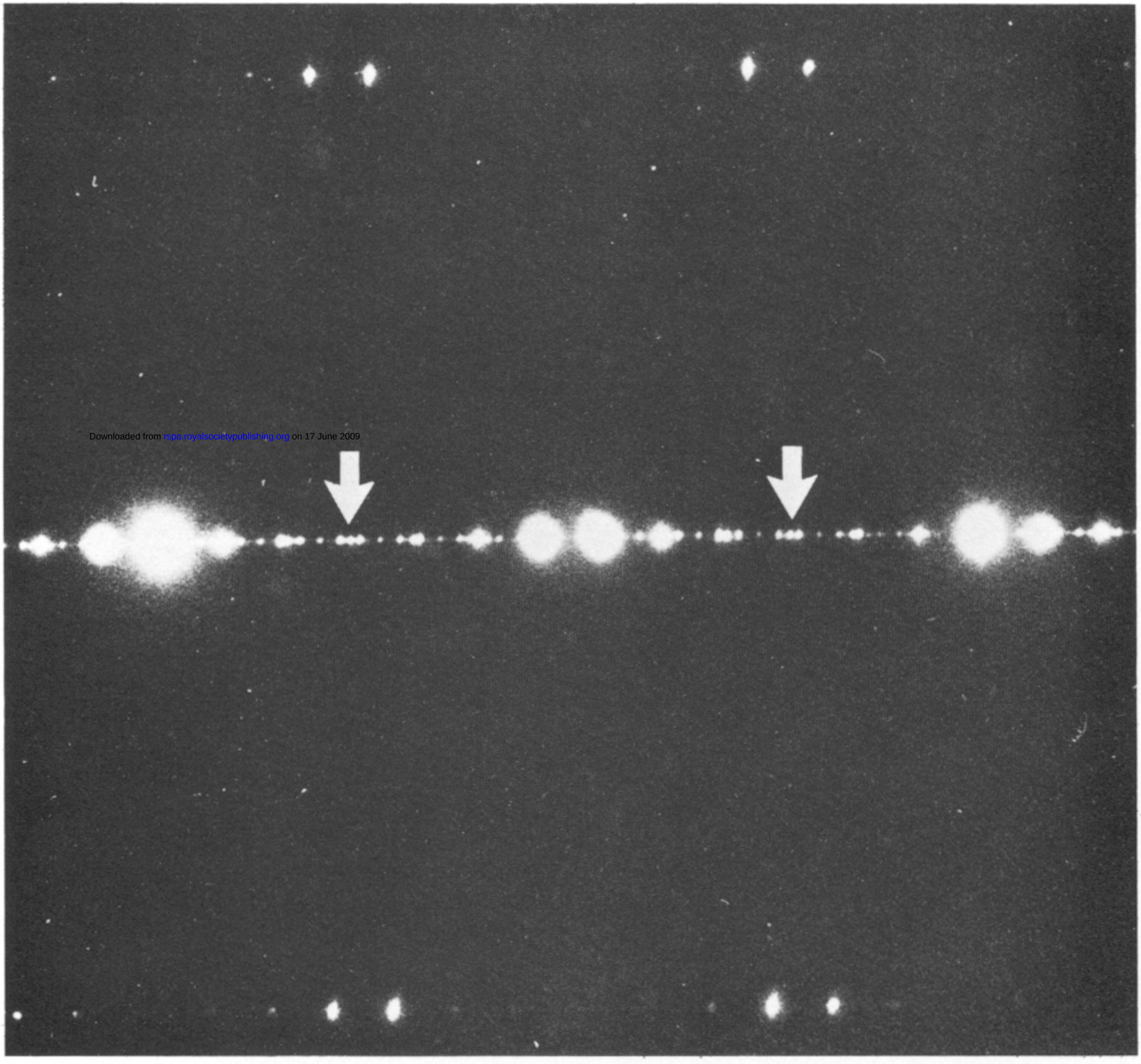

FIGURE 14. Satellites accompanying the superlattice spots in a crystal of $Bi_{0.1}WO_3$ (nominal). The overall periodicity of the satellite spot spacing corresponds to *ca.* 16 nm. The pattern corresponds to [011] projection.